J. Fluid Mech. (2001), *vol.* 426, *pp.* 95–133. Printed in the United Kingdom

© 2001 Cambridge University Press

Disturbing vortices

By N. J. BALMFORTH[1], STEFAN G. LLEWELLYN SMITH[2] AND W. R. YOUNG[3]

[1]Department of Applied Mathematics and Statistics, University of California, Santa Cruz, CA 95064, USA

[2]Department of Mechanical and Aerospace Engineering, University of California, San Diego, CA 92093-0411, USA

[3]Scripps Institution of Oceanography, University of California, San Diego, CA 92093-0230, USA

(Received 14 December 1999 and in revised form 11 July 2000)

Inviscid spatially compact vortices (such as the Rankine vortex) have discrete Kelvin modes. For these modes, the critical radius, at which the rotation frequency of the wave matches the angular velocity of the fluid, lies outside the vortex core. When such a vortex is not perfectly compact, but has a weak vorticity distribution beyond the core, these Kelvin disturbances are singular at the critical radius and become 'quasi-modes'. These are not true eigenmodes but have streamfunction perturbations that decay exponentially with time while the associated vorticity wraps up into a tight spiral without decay. We use a matched asymptotic expansion to derive a simplified description of weakly nonlinear, externally forced quasi-modes.

We consider the excitation and subsequent evolution of finite-amplitude quasi-modes excited with azimuthal wavenumber 2. Provided the forcing amplitude is below a certain critical amplitude, the quasi-mode decays and the disturbed vortex returns to axisymmetry. If the amplitude of the forcing is above critical, then nonlinear effects arrest the decay and cat's eye patterns form. Thus the vortex is permanently deformed into a tripolar structure.

1. Introduction

The development of non-axisymmetric perturbations on a stable vortex is a classical problem in fluid mechanics and needs little introduction. The exploration of perturbed vortices began with Rayleigh (1880) and Kelvin (1880). But recent works show that certain aspects of even the linear problem are still not entirely resolved (Bernoff & Lingevitch 1994; Lingevitch & Bernoff 1995; Montgomery & Kallenbach 1997; Bassom & Gilbert 1998; Schecter *et al.* 1999; Schecter 1999). These studies explore the linear theory of *axisymmetrization*. The issue is whether the streamfunction of a perturbed, stable vortex will eventually return to axisymmetry as a result of the tight spiral winding of non-axisymmetrical structure in vorticity. In this regard, Bassom & Gilbert (1998) show that the streamfunction of a linearly perturbed Gaussian vortex returns to axisymmetry via an inviscid algebraic decay. But it is only the streamfunction which relaxes to axisymmetry: the vorticity perturbation is wound up without decay in amplitude. The algebraic decay of the streamfunction is a result of the coarse-graining or averaging effect of the inverse Laplacian operator on the increasingly finely scaled vorticity.

However, axisymmetry cannot be the universal fate of all linear perturbations

https://doi.org/10.1017/S0022112000002159 Published online by Cambridge University Press

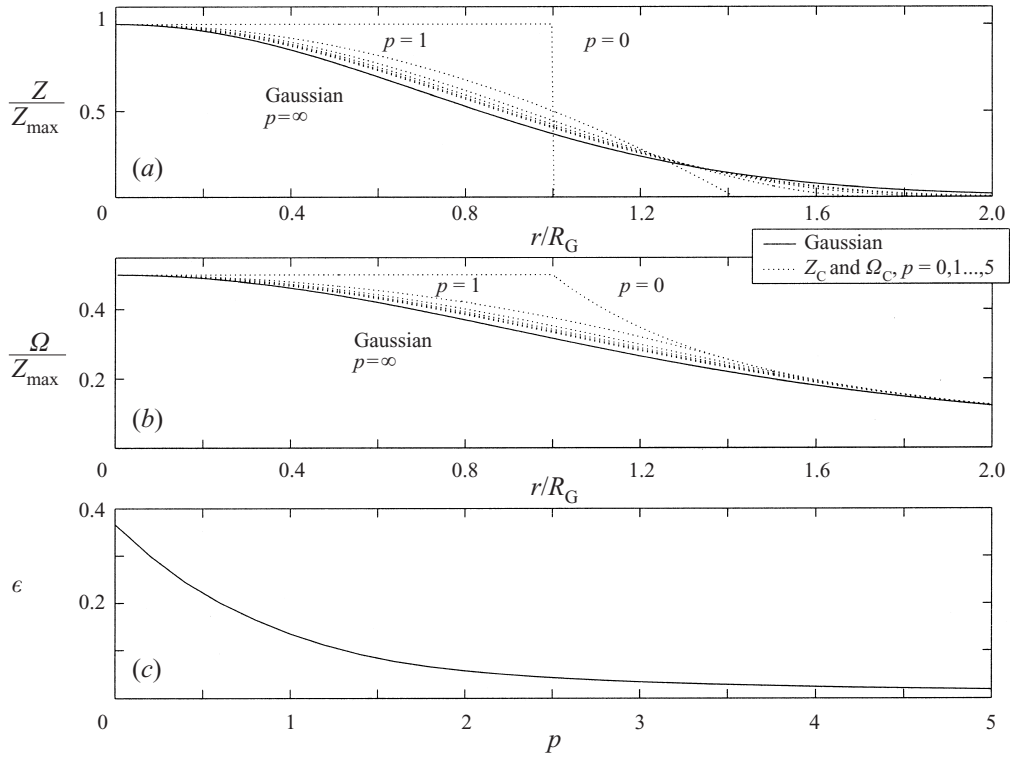


FIGURE 1. The family of compact vortices (defined in (2.3)) that approximate the Gaussian vortex (with vorticity $Z_G = Z_{max} \exp(-r^2/R_G^2)$). (*a*) Vorticity, Z/Z_{max}, and (*b*) the scaled angular velocity, Ω/Z_{max}, for p between 0 and 5. The Gaussian vortex corresponds formally to $p \to \infty$. (*c*) The small parameter ϵ defined in (2.14) as a function of p.

to all vortices. In particular, spatially compact vortices† may support wave-like disturbances riding on the vortex rim, or *Kelvin modes*. The streamfunction of a linearly perturbed compact vortex never returns to axisymmetry because these Kelvin modes are undamped. The best known example of Kelvin modes is provided by the Rankine or top-hat vortex (Batchelor 1967). The persistently non-axisymmetric vortices seen in contour dynamic calculations of Dritschel (1998) exemplify these undamped disturbances in the fully nonlinear regime.

It is irritating that conclusions concerning important physical issues, such as the long-term relaxation of the streamfunction to axisymmetry, seem to turn on fussy mathematical restrictions concerning the smoothness or compactness of the vorticity profile. For example, the Gaussian vortex can be closely approximated by smooth compact vortices (see figure 1) and so it seems unreasonable that there can be any real physically important difference between the evolution of perturbations on a Gaussian vortex and one of its close approximants. Part of our purpose is to understand how the two can differ so.

In addition to theoretical issues, an important motivation for this paper comes from experiments with non-neutral plasmas (Driscoll & Fine 1990; Gould 1994; Cass 1998) and rapidly rotating fluids (van Heijst, Kloosterziel & Williams 1991), both of which

† By a 'compact' vortex we mean that the vorticity is zero outside some radius R. A 'top-hat' vortex is compact, but a Gaussian vortex is non-compact.

https://doi.org/10.1017/S0022112000002159 Published online by Cambridge University Press

provide laboratory analogues for two-dimensional fluid mechanics. In these contexts, it is possible to study perturbations by, for example, briefly imposing an external irrotational flow that elliptically distorts an axisymmetrical vortex. Disturbances then have finite amplitude, and the evolution of nonlinear perturbations is not necessarily predicted by linear theory.

The importance of nonlinear effects is clearly illustrated by analogous problems in plasma physics, where the decay of the streamfunction has an analogue in the Landau damping of the electric field. In that subject, it is a widely accepted view that perturbations of sufficient amplitude do not decay back to the undisturbed state (Sugihara & Kamimura 1972; Feix, Bertrand & Ghizzo 1994; Manfredi 1997). Instead the disturbance excites a finite-amplitude wave, known in plasma physics as a BGK-mode (Bernstein, Greene & Kruskal 1958). The main results of this article are to show that nonlinearity also operates to arrest the decay of streamfunction perturbations on a fluid vortex (as suggested by numerical simulations, e.g. Rossi, Lingevitch & Bernoff 1997; Möller & Montgomery 1999), and to estimate the threshold amplitude. The analogue of the BGK-mode is a cat's eye structure which, in the case of an elliptical perturbation, takes the form of a tripole, as seen in experiments (van Heijst *et al.* 1991; Cass 1998). The formation of these structures highlights the inadequacy of linear theory. Rather, the outstanding issue is to determine the threshold amplitude that must be exceeded in order to form a multipole.

The approach we follow in this article is to construct compact approximations to smooth, non-compact vortices. The compact approximant possesses a Kelvin mode although the smooth vortex does not. Thus, we follow an asymptotic route to understand how the Kelvin mode disappears as the compact vortex is deformed into a non-compact structure. This perturbation scheme shows that the Kelvin mode is replaced by a *quasi-mode* (see also Briggs, Daugherty & Levy 1970). In linear theory, a quasi-mode is a special solution of the initial-value problem in which the streamfunction decays exponentially, but the vorticity inexorably wraps into a filamentary spiral without decay.

The strategy is illustrated in figure 1. There, we replace the Gaussian vortex by a family of compact approximants. The magnitude of the error is small (see panel *c*) and provides us with a small parameter with which we can organize an asymptotic expansion. With a suitable scaling of the amplitude of the disturbance we can simultaneously capture finite-amplitude effects and derive a weakly nonlinear description of the Kelvin quasi-mode.

Although our focus is on externally perturbed stable vortices, the mathematical approach is much like weakly nonlinear theories of marginally unstable normal modes in ideal shear flows (Stewartson 1981; Churilov & Shukhman 1987; Goldstein & Leib 1988). A unifying feature of these weakly nonlinear expansions is an apparent singularity of the linear theory, known as the 'critical level'. For the vortex, the singularity occurs at the radius where the rotation rate matches the rotation frequency of a Kelvin mode. We refer to this radius as the critical radius. The singularity is an unphysical artifact of inviscid linear theory, and signals the need to include additional physics in a slender region surrounding the critical radius. This annular region is the critical 'layer'. Within the critical layer, without viscosity, the vorticity develops on an increasingly fine scale. To capture these details we develop an asymptotic expansion outside the critical layer which recapitulates the normal-mode solution. The critical-level singularity in this 'outer' solution is then healed by finding an 'inner' solution within the critical layer. The two solutions must be matched together in order to complete the reduction of the problem. The recipe is therefore a matched asymptotic

https://doi.org/10.1017/S0022112000002159 Published online by Cambridge University Press

expansion. A parallel approach is taken by Le Dizès (2000). The main difference between the two approaches is the role of viscosity which is sufficiently strong in Le Dizès's analysis to render the critical layer quasi-steady. By contrast, we ignore viscosity completely and develop a theory of non-steady, critical layers.

2. Formulation

2.1. *The equations*

In ideal fluid theory, any circular vortex with rotation rate $\Omega(r)$ and vorticity $Z(r) = r\Omega' + 2\Omega$ is a possible equilibrium. Here, we confine attention to stable vortices for which $\Omega(r)$ and $Z(r)$ are monotonically non-increasing functions of the radius r. In polar coordinates (r, θ), the Euler equation governing perturbations to such a basic state is

$$r\zeta_t + \Omega r\zeta_\theta - (\psi_\theta + \psi^{\rm ext}_\theta)Z' + \frac{\partial(\psi + \psi^{\rm ext}, \zeta)}{\partial(r, \theta)} = 0. \tag{2.1}$$

In (2.1), the disturbance vorticity ζ and the disturbance streamfunction ψ are related by

$$\zeta = \psi_{rr} + r^{-1}\psi_r + r^{-2}\psi_{\theta\theta}. \tag{2.2}$$

Also in (2.1), $\psi^{\rm ext}(x, y, t)$ is an externally imposed, irrotational ($\nabla^2\psi^{\rm ext} = 0$) streamfunction which models the perturbing influence of distant vortices or boundary conditions. $\psi^{\rm ext}$ azimuthally disturbs the basic-state vorticity distribution $Z(r)$; the issue is how, or if, such a perturbation relaxes back to axisymmetry. We solve these equations on the infinite domain, $r \in [0, \infty)$ and $0 \leqslant \theta \leqslant 2\pi$, subject to the boundary conditions, $\psi_r \to 0$ and $\zeta \to 0$ as $r \to \infty$, regularity at the origin and periodicity in θ.

2.2. *Compact vortices*

We begin by considering a special class of basic-state vortices, namely 'compact vortices', for which $Z(r) = 0$ if $r > R_{\rm C}$. We refer to $R_{\rm C}$ as the 'edge' of the compact vortex. These compact vortex profiles will be used to approximate extended smooth vortices such as the Gaussian, $Z_{\rm G}(r) \equiv Z_{\max}\exp(-r^2/R_{\rm G}^2)$. The latter have no sharp edge, but their vorticity distribution has a characteristic radial length scale, such as $R_{\rm G}$.

Though we develop the theory for a general compact vortex, as a specific illustration it is helpful to consider the family defined by

$$Z_{\rm C}(r) = Z_{\max}\begin{cases} [1 - (r/R_{\rm C})^2]^p & \text{if } 0 < r < R_{\rm C}, \\ 0 & \text{if } R_{\rm C} < r. \end{cases} \tag{2.3}$$

The rotation rate of the family is given by

$$\Omega_{\rm C}(r) = \frac{\Gamma}{2\pi r^2}\begin{cases} 1 - [1 - (r/R_{\rm C})^2]^{p+1} & \text{if } 0 < r < R_{\rm C}, \\ 1 & \text{if } R_{\rm C} < r, \end{cases} \tag{2.4}$$

where the total circulation is

$$\Gamma \equiv 2\pi\int_0^\infty Z_{\rm C}(r) r\,{\rm d}r = \frac{\pi Z_{\max} R_{\rm C}^2}{p+1}. \tag{2.5}$$

The special case $p = 0$ is the well known Rankine vortex. If $p \to \infty$ with

$$R_{\rm C} = R_{\rm G}\sqrt{p+1}, \tag{2.6}$$

https://doi.org/10.1017/S0022112000002159 Published online by Cambridge University Press

then Z_C limits to the non-compact Gaussian vortex $Z_G = Z_{max}\exp(-r^2/R_G^2)$ (see figure 1). In other words, we prescribe the family of compact approximants so that the circulation and peak vorticity are independent of p and equal to those of the Gaussian.

2.3. *The Kelvin modes of compact vortices*

Compact vortices sometimes possess 'Kelvin modes' (and sometimes they do not). This means that if we linearize (2.1) and look for modal solutions,

$$[\psi(r,\theta,t),\zeta(r,\theta,t)] = [f(r),g(r)]\exp[im(\theta-\omega_m t)], \quad g \equiv f'' + r^{-1}f' - m^2 r^{-2}f, \tag{2.7}$$

then the eigenproblem for ω_m,

$$(\Omega_C - \omega_m)rg = Z_C' f, \tag{2.8}$$

sometimes has solutions for which the critical radius r_m, defined implicitly by

$$\omega_m = \Omega_C(r_m) \qquad \text{(definition of } r_m\text{)}, \tag{2.9}$$

satisfies $r_m > R_C$.

The Rankine or top-hat vortex, $p = 0$ in (2.3), provides the simplest illustration of a vortex with Kelvin modes. The modal solution of (2.7) and (2.8) is

$$\omega_m = \left(\frac{m-1}{2m}\right)Z_{max}, \qquad r_m = R_C\sqrt{\frac{m}{m-1}} > R_C. \tag{2.10}$$

Thus, for all azimuthal wavenumbers m, the critical radius r_m is in the domain $r > R_C$ where the Rankine vortex has $Z_C(r) = 0$. The eigenfunctions which accompany ω_m in (2.9) are

$$f_m(r) = \left(\frac{r_m}{R_C}\right)^m \begin{cases} (r/R_C)^m & \text{if } r < R_C, \\ (r/R_C)^{-m} & \text{if } r > R_C, \end{cases} \quad \text{and} \quad g_m(r) = -\left(\frac{r_m}{R_C}\right)^m \frac{2m}{R_C}\delta(r-R_C). \tag{2.11}$$

The factor $(r_m/R_C)^m$ is included so that the eigenmode satisfies the normalization condition $f(r_m) = 1$. The eigenfunctions above have a singularity at $r = R_C$ which corresponds to the discontinuity in the vorticity of the basic state at $r = R_C$. But there is no singularity at the critical radius, r_m.

For general vortices, the streamfunction $f(r)$ contains both regular and singular Frobenius solutions at the critical radius: $f_{reg} = (r-r_m)+\cdots$ and $f_{sing} = 1+Z'(r_m)(r-r_m)\log|r-r_m|+\cdots$, respectively. Moreover, a standard construction shows that the regular solution alone cannot satisfy the boundary conditions. Compact vortices may avoid the irregularity in f_{sing} if $r_m > R_C$ because $Z_C'(r_m) = 0$. These are the Kelvin modes. In this case, 'The disturbing infinity in Lord Rayleigh's solution' noted by Kelvin in 1880 (and now known as the critical-level singularity) has no effect on the dynamics.

At this point we have shown that the Rankine vortex ($p = 0$) has a Kelvin mode for every value of m yet the Gaussian vortex ($p = \infty$) has only a trivial Kelvin mode with $m = 1$ (for a discussion of this $m = 1$ translation mode see Bernoff & Lingevitch 1994). It is natural to enquire how the Kelvin modes disappear as p increases from zero to infinity. We solve the eigenvalue problem by numerical means in order to determine when these modes disappear, and we find that Kelvin modes exist the (m,p)-plane only below the curve in figure 2. Notice that the vortex with $p = 1$,

https://doi.org/10.1017/S0022112000002159 Published online by Cambridge University Press

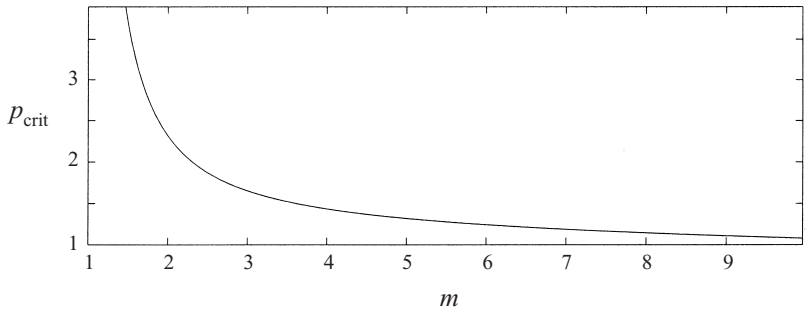


FIGURE 2. The family of compact vortices $Z_{\rm C}$ in (2.3) has a Kelvin mode with azimuthal wavenumber m in the region below the curve. For computational purposes, the azimuthal wavenumber m has been treated as a continuous variable.

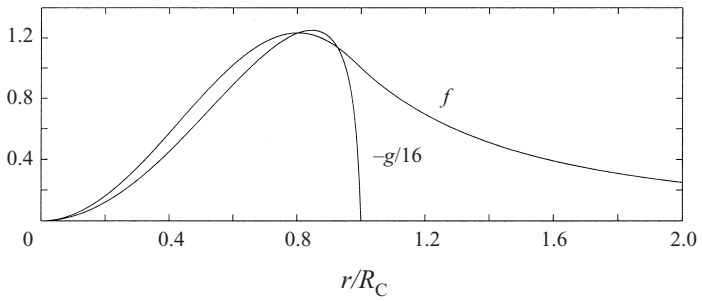


FIGURE 3. Streamfunction and vorticity eigenfunctions f and g for the $p = 2$ member of the family (2.3). The azimuthal wavenumber is $m = 2$ and the eigenfunction f is normalized so that $f(r_2) = 1$ where $r_2 = 1.027R_{\rm C}$ is the critical radius of the $m = 2$ mode.

like that for $p = 0$, possesses a full set of Kelvin modes. But if $p > 1$ then Kelvin modes exist only when p is less than some cut-off; the cut-off is the curve $p = p_{\rm crit}(m)$ displayed in figure 2. As p increases, mode m disappears when the critical radius r_m first encounters the edge of the compact vortex at $r = R_{\rm C}$.†

2.4. *The $m = 2$ Kelvin mode of the $p = 2$ vortex*

As an illustration of the Kelvin modes which exist on compact vortices with smooth edges we consider the $m = 2$ Kelvin mode of the $p = 2$ vortex. Numerical calculations locate an $m = 2$ Kelvin mode solution with $\omega_2 = 0.1571Z_{\rm max}$ and $r_2 = 1.027R_{\rm C}$, which shows that the critical radius is only slightly outside the edge of the $p = 2$ vortex.

Figure 3 shows the functions $f(r)$ and $g(r)$ defined in (2.7); the vorticity eigenfunction g is non-zero only in the region $0 < r < R_{\rm C}$ where $Z_{\rm C}(r) \neq 0$. We use a frame which is corotating with the modal disturbance so that the new azimuthal coordinate is $\vartheta \equiv \theta - \omega_2 t$. If $\Psi_{\rm C}(r)$ is the streamfunction of the vortex in the original frame, then in the ϑ-frame the total streamfunction is

$$\psi(r, \vartheta) = \Psi_{\rm C}(r) - \tfrac{1}{2}\omega_2 r^2 + \tfrac{1}{200}R_{\rm C}^2 Z_{\rm max} f(r)\cos(2\vartheta). \tag{2.12}$$

The factor $R_{\rm C}^2 Z_{\rm max}$ is included for dimensional consistency and the fraction, $1/200$, on purely aesthetic grounds to ensure that there is, visually, a strong distortion of

† A similar phenomenon arises in shear flow in channels: broken-line profiles have discrete modes, but smooth shears typically do not, so as one smooths out the broken lines, the discrete modes must merge with the continuum.

https://doi.org/10.1017/S0022112000002159 Published online by Cambridge University Press

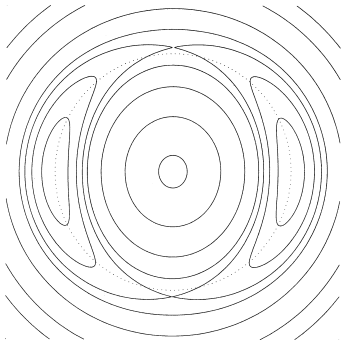


FIGURE 4. Total streamfunction in (2.12); the dotted circle shows the edge of the compact vorticity distribution of the basic state.

the basic-state vortex by the $m = 2$ mode (see figure 4). The distorted vortex has a tripolar structure (Driscoll & Fine 1990; van Heijst *et al.* 1991).

2.5. *Skirted vortices*

Our main goal is to determine how the Kelvin mode of a compact vortex becomes excited by external forcing, and how that mode is affected if a small amount of vorticity is introduced near the critical radius r_m. We address these issues by adding a small, non-compact, axisymmetric vorticity perturbation to a compact vortex. We refer to the small additional vorticity, which creates a dynamically important critical layer at r_m, as a 'skirt'.

Thus, if $Z_C(r)$ and $\Omega_C(r)$ denote the vorticity and rotation rate of a compact vortex, then the new profile is

$$Z(r) = Z_C(r) + \epsilon Z_S(r), \qquad \Omega(r) = \Omega_C(r) + \epsilon \Omega_S(r), \tag{2.13}$$

where $Z_S(r)$ and $\Omega_S(r)$ are the skirt profiles. The small parameter ϵ is defined so that

$$\max_r Z_S(r) = Z_{\max} \qquad \text{(definition of } \epsilon\text{)}. \tag{2.14}$$

Figure 1 shows that the Gaussian vorticity profile, $Z_G = Z_{\max} \exp(-r^2/R_G^2)$, can be represented as the sum of a dominant compact vortex and a smaller skirt. Specifically, in figure 1, where $p = 0$ to 5, one has $\epsilon = 0.366$, 0.135, 0.057, and so on.

However, in fact, we are unable to make the error arbitrarily small: the perturbation scheme in § 3 is founded on the existence of a Kelvin wave to leading order. If we take p to be too large, that mode disappears. Hence, the precision of the perturbation expansion has a limit. For $m = 2$, we cannot take p to exceed a value much above 2, and so our small parameter is 0.057 or more. Perhaps other forms for the compact approximant would work better than the particular family used here and furnish smaller values for ϵ, but we have not explored this any further.

3. The expansion

In this section we consider a compact vortex which has an $m = 2$ Kelvin mode with a critical radius at $r = r_2$. With the addition of a small skirt there is then a dynamically consequential singularity at critical radius r_2. As a direct consequence, the Kelvin mode ceases to exist as a true eigenmode of the vortex. Instead, the disturbance that at leading order resembles the original Kelvin mode begins to wrap

https://doi.org/10.1017/S0022112000002159 Published online by Cambridge University Press

up the vorticity distribution of the skirt in a thin region surrounding the critical ring. The goal of the expansion is to focus attention on the neighbourhood of r_2 and obtain a simplified description of this critical layer. Whilst the details are different, the procedure is similar to the matching calculation performed by Benney & Bergeron (1969) for inviscid shears, and to the forced critical layer problem of Stewartson (1978) and Warn & Warn (1978). The problem also shares the same philosophy as the division of a plasma into non-resonant and resonant electrons in the single-wave model of O'Neil, Winfree & Malmberg (1971; see also O'Neil 1965, and Imamura, Sugihara & Taniuti 1969).

To ease the exposition we develop the expansion for the special case $m = 2$. There is no essential difficulty in repeating the calculation with other azimuthal wavenumbers $m > 2$. However the first azimuthal mode, $m = 1$, differs essentially from the others because it describes, in part, the translation of the vortex as a whole. In fact, when the $m = 1$ components of $\psi^{\rm ext}$ are irrotational, this part of the disturbance is removed exactly by changing the frame of reference (Bernoff & Lingevitch 1994).

The expansion is launched by throwing (2.13) into (2.1) and making the additional scaling assumptions that

$$[\psi(r,\theta,t),\zeta(r,\theta,t)] \to \epsilon^2[\psi(r,\vartheta,\tau),\zeta(r,\vartheta,\tau)], \qquad \psi^{\rm ext}(r,\theta,t) \to \epsilon^3\psi^{\rm ext}(r,\vartheta,\tau). \tag{3.1}$$

In (3.1) we have also changed frame so that the coordinate system is corotating with the speed of the compact vortex at r_2:

$$\vartheta \equiv \theta - \omega_2 t, \qquad \tau = \epsilon t. \tag{3.2}$$

The variables now depend only on the slow time τ, so we assume that the change of frame in the definition of ϑ absorbs the fast time dependence. The scaling assumptions in (3.1) and (3.2) ensure that the nonlinear terms appear at the same order as the external forcing.

The scaled equations of motion are

$$\epsilon r\zeta_\tau + (\tilde{\Omega}_{\rm C} + \epsilon\Omega_{\rm S})r\zeta_\vartheta - (\psi_\vartheta + \epsilon\psi^{\rm ext}_\vartheta)(Z'_{\rm C} + \epsilon Z'_{\rm S}) + \epsilon^2\frac{\partial(\psi + \epsilon\psi^{\rm ext},\zeta)}{\partial(r,\vartheta)} = 0. \tag{3.3}$$

In (3.3),

$$\tilde{\Omega}_{\rm C}(r) \equiv \Omega_{\rm C}(r) - \Omega_{\rm C}(r_2) \tag{3.4}$$

is, to leading order, the rotation rate in new frame.

We assume that the external perturbation has the irrotational form

$$\psi^{\rm ext} = r^2[\hat{b}(\tau)e^{2{\rm i}\vartheta} + \hat{b}^*(\tau)e^{-2{\rm i}\vartheta}]. \tag{3.5}$$

This ensures that the $m = 2$ Kelvin mode of the leading-order vortex is excited by the irrotational flow of a distant vorticity field. Note that we have taken the forcing to rotate with the angular pattern speed of the Kelvin wave. This is not essential and we could introduce a Fourier decomposition of a general forcing. The point is that, at the weak forcing amplitudes used in the expansion (order ϵ^3), only the components which are 'resonant' matter. Hence we simply take the form (3.5) and ignore the non-resonant components.

The solution $[\psi,\zeta]$ of (3.3) is now expanded in the sequences

$$\psi = \psi^0 + \epsilon\psi^1 + \cdots, \qquad \zeta = \zeta^0 + \epsilon\zeta^1\cdots. \tag{3.6}$$

https://doi.org/10.1017/S0022112000002159 Published online by Cambridge University Press

3.1. *The outer solution at leading order*

On substituting (3.6) into (3.3), the leading-order equation is

$$\tilde{\Omega}_{\mathrm{C}} r \zeta^0_\vartheta = Z'_{\mathrm{C}} \psi^0_\vartheta, \tag{3.7}$$

with the solution,

$$[\psi^0, \zeta^0] = a[f, g], \qquad a(\vartheta, \tau) \equiv \hat{a}(\tau) \mathrm{e}^{2\mathrm{i}\vartheta} + \hat{a}^*(\tau) \mathrm{e}^{-2\mathrm{i}\vartheta}. \tag{3.8}$$

In (3.8), $\hat{a}(\tau)$ is the amplitude of the Kelvin eigenmode of the compact vortex Z_{C}. The leading-order streamfunction evaluated at r_2 will appear prominently in the final reduced description, and so it is convenient to normalize the eigenfunction $f(r)$ with $f(r_2) = 1$. With this convention, $\psi^0(r_2, \vartheta, \tau) = a(\vartheta, \tau)$.

Our amplitude $\hat{a}(\tau)$ is not yet determined, but we follow the usual path of asymptotics: we proceed to higher order with the aim of enforcing a solvability condition on the next-order corrections. This has two effects: solvability ensures that the asymptotic ordering of the solution remains intact, and the solvability condition, the Fredholm Alternative, provides the evolution equation for $\hat{a}(\tau)$. In the present case, however, there are some subtleties in the theory that significantly enrich the asymptotic description. These originate completely as a result of critical-radius singularity.

3.2. *The outer solution at order* ϵ

At the next order, one has

$$\tilde{\Omega}_{\mathrm{C}} \mathscr{M} \psi^1_\vartheta = -r\zeta^0_\tau - \Omega_{\mathrm{S}} r \zeta^0_\vartheta + Z'_{\mathrm{S}} \psi^0_\vartheta + Z'_{\mathrm{C}} \psi^{\mathrm{ext}}_\vartheta, \tag{3.9}$$

where $\mathscr{M}$ is the self-adjoint operator

$$\mathscr{M} \equiv \partial_r r \partial_r - r^{-1} \partial^2_\vartheta - \tilde{\Omega}^{-1}_{\mathrm{C}} Z'_{\mathrm{C}}. \tag{3.10}$$

(Because $Z_{\mathrm{C}}(r_2) = 0$, the coefficient $\tilde{\Omega}^{-1}_{\mathrm{C}} Z'_{\mathrm{C}}$ in (3.10) is non-singular.) Note that $\mathscr{M} f = 0$.

Equation (3.9) is where problems with solvability arise; this equation has singular solutions and these must be avoided by fixing the evolutionary behaviour of $\hat{a}(\tau)$. With the Fredholm alternative in sight, one multiplies (3.9) by $\tilde{\Omega}^{-1}_{\mathrm{C}}(r)$. At this juncture, one must be sensitively aware that $\tilde{\Omega}_{\mathrm{C}}(r_2) = 0$. Consequently, the resulting right-hand side contains a critical-level singularity associated with the skirt vorticity gradient. The physical interpretation of this singularity is that the external forcing excites a disturbance that to leading order takes the form of the Kelvin wave. But this disturbance wraps up the skirt vorticity gradient over a slender annulus surrounding the critical radius. In the fashion of a resonant response, this action generates a compact vorticity distribution that appears singular outside the annular region. We capture the effect explicitly by writing

$$\mathscr{M} \psi^1_\vartheta = -\tilde{\Omega}^{-1}_{\mathrm{C}} [r\zeta^0_\tau + \Omega_{\mathrm{S}} r \zeta^0_\vartheta - Z'_{\mathrm{S}} \psi^0_\vartheta - Z'_{\mathrm{C}} \psi^{\mathrm{ext}}_\vartheta] + \rho(\vartheta, \tau) r_2 \delta(r - r_2), \tag{3.11}$$

where the final term in (3.11), $\rho(\vartheta, \tau) r_2 \delta(r - r_2)$, is a formal device to represent the concentrated vorticity at the critical radius r_2. This concentration is resolved separately in the annular critical layer using a different expansion, given below. Notice that $\rho(\vartheta, \tau)$ is the only term on the right-hand side of (3.11) containing azimuthal harmonics other than $m = 2$.

The solution of (3.11) can be represented as

$$[\psi^1(r, \vartheta, \tau), \rho(\vartheta, \tau)] = \sum_{m=-\infty}^{\infty} \mathrm{e}^{\mathrm{i}m\vartheta} [\psi^1_m(r, \tau), \rho_m(\tau)]. \tag{3.12}$$

https://doi.org/10.1017/S0022112000002159 Published online by Cambridge University Press

If $m \neq 2$ then projecting (3.11) onto $\exp(\mathrm{i}m\vartheta)$ gives

$$\mathscr{M}_m \psi_m^1 = -\mathrm{i}m^{-1}\rho_m r_2 \delta(r - r_2), \tag{3.13}$$

where $\mathscr{M}_m$ is $\mathscr{M}$ in (3.10) with $\partial_\vartheta \to \mathrm{i}m$. Once $\rho(\vartheta, \tau)$ is obtained with an analysis of the critical layer, there is no difficulty in solving (3.13) because $\mathscr{M}_m$ (with $m \neq 2$) has no non-trivial null functions. Thus, the terms with $m \neq 2$ in (3.12) are a passive response of the outer flow to the concentrated vorticity in the critical layer.

3.3. *The resonant terms at order* ϵ

The resonant harmonic in (3.11) is $m = 2$; projecting onto $\exp(2\mathrm{i}\vartheta)$ gives

$$\mathscr{M}_2 \psi_2^1 = \tilde{\Omega}_\mathrm{C}^{-1}[\tfrac{1}{2}\mathrm{i}rg\hat{a}_\tau - r\Omega_\mathrm{S} g\hat{a} + Z_\mathrm{S}' f\hat{a} + Z_\mathrm{C}' r^2 \hat{b}] - \tfrac{1}{2}\mathrm{i}\rho_2 r_2 \delta(r - r_2). \tag{3.14}$$

To obtain (3.14) we have used the form of ψ^{ext} in (3.5) and ψ^0 in (3.8).

Because $g(r_2) = 0$, the right-hand side of (3.14) has only two singularities: the $\delta(r - r_2)$, and the pole $(r - r_2)^{-1}$ in the term $\tilde{\Omega}_\mathrm{C}^{-1} Z_\mathrm{S}' f\hat{a}$. These singularities prevent a blithe application of the Fredholm Alternative to (3.14). Instead, we rewrite (3.14) as

$$\mathscr{M}_2 \psi_2^1 = \mathscr{R} + \frac{r_2 \mu_2 f}{r - r_2}\hat{a} - \tfrac{1}{2}\mathrm{i}\rho_2 r_2 \delta(r - r_2), \tag{3.15}$$

where the constant μ_2 is

$$\mu_2 \equiv Z_\mathrm{S}'(r_2)/r_2 \tilde{\Omega}_\mathrm{C}'(r_2). \tag{3.16}$$

The non-singular terms on the right-hand side of (3.15) are collected in

$$\mathscr{R} \equiv \tilde{\Omega}_\mathrm{C}^{-1}[(\mathrm{i}/2)rg\hat{a}_\tau - r\Omega_\mathrm{S} g\hat{a} + Z_\mathrm{C}' r^2 \hat{b}] + \left[\frac{Z_\mathrm{S}'}{\tilde{\Omega}_\mathrm{C}} - \frac{r_2\mu_2}{r - r_2}\right] f\hat{a}. \tag{3.17}$$

In anticipation of the matching problem, we extract two properties of ψ_2^1 from (3.15) and (3.17). First, it follows from (3.15) that in the neighbourhood of r_2, ψ_2^1 has the form

$$\psi_2^1(r, \vartheta, \tau) \approx \psi_2^1(r_2, \vartheta, \tau) + \mu_2 (r - r_2) \ln|r - r_2| \hat{a} + (r - r_2) \begin{cases} c^- & \text{if } r < r_2, \\ c^+ & \text{if } r > r_2. \end{cases} \tag{3.18}$$

The neglected terms in the expansion (3.18) are $O[(r - r_2)^2 \ln|r - r_2|]$.

Next, using a variant of the Fredholm procedure, we can calculate $c^+ - c^-$. To do this, take $r^- < r_2 < r^+$ and form the combination

$$\left[\int_0^{r^-} + \int_{r^+}^{\infty}\right] f \times (3.15)\,\mathrm{d}r. \tag{3.19}$$

On taking the limits $r^- \uparrow r_2$ and $r^+ \downarrow r_2$, one finds

$$c^+ - c^- = -r_2^{-1} \int_0^\infty f\mathscr{R}\,\mathrm{d}r - \mu_2 \hat{a} \mathscr{P}\int_0^\infty \frac{f^2}{r - r_2}\,\mathrm{d}r, \tag{3.20}$$

where the principal part integral in (3.20) is

$$\mathscr{P}\int_0^\infty \frac{f^2}{r - r_2}\,\mathrm{d}r \equiv \lim_{r^\pm \to r_2} \left\{ \left[\int_0^{r^-} + \int_{r^+}^\infty\right] \frac{f^2}{r - r_2}\,\mathrm{d}r - \ln\left|\frac{r^- - r_2}{r^+ - r_2}\right| \right\}. \tag{3.21}$$

The integral above is independent of the fashion in which r^+ and r^- approach r_2. (It is convenient, but not essential, to obtain a standard principal part by taking the limit with $r_2 - r^- = r^+ - r_2$.)

https://doi.org/10.1017/S0022112000002159 Published online by Cambridge University Press

On substituting the definition of $\mathscr{R}$ in (3.17) into (3.20) and rearranging, we find

$$\mathrm{i}\mathscr{I}_1\hat{a}_\tau + (\mathscr{I}_2 + \mathscr{I}_3 + \mathscr{I}_4)\hat{a} = \mathscr{I}_5\hat{b} + (c^+ - c^-), \tag{3.22}$$

where

$$\mathscr{I}_1 \equiv -\int_0^{R_C} \frac{rfg}{2r_2\tilde{\Omega}_C}\,\mathrm{d}r, \quad \mathscr{I}_2 \equiv \int_0^{R_C} \frac{r\Omega_S fg}{r_2\tilde{\Omega}_C}\,\mathrm{d}r, \quad \mathscr{I}_5 \equiv \int_0^{R_C} \frac{r^2 f Z_C'}{r_2\tilde{\Omega}_C}\,\mathrm{d}r, \tag{3.23}$$

and

$$\mathscr{I}_3 \equiv -\int_0^{\infty} \left(\frac{Z_S'}{r_2\tilde{\Omega}_C} - \frac{\mu_2}{r - r_2}\right) f^2\,\mathrm{d}r, \quad \mathscr{I}_4 \equiv -\mu_2 \mathscr{P}\int_0^{\infty} \frac{f^2}{r - r_2}\,\mathrm{d}r. \tag{3.24}$$

By using $f/\tilde{\Omega}_C = rg/Z_C'$, one can show that $\mathscr{I}_1 > 0$. To obtain an expression for the jump, $c^+ - c^-$, in (3.22) we turn to an analysis of the critical layer at r_2.

3.4. *The critical layer at r_2*

In the inner region, an appropriate radial variable is

$$Y \equiv \epsilon^{-1}(r - r_2). \tag{3.25}$$

The expansion of the streamfunction is

$$\psi = \psi^0(r_2, \vartheta, \tau) + \epsilon[\psi^1(r_2, \vartheta, \tau) + Y\psi_r^0(r_2, \vartheta, \tau)] + \epsilon^2 \ln\epsilon\,\mu_2 Y\psi^0(r_2, \vartheta, \tau) + \epsilon^2[\phi + \tfrac{1}{2}Y^2\psi_{rr}^0(r_2, \vartheta, \tau)] + \cdots. \tag{3.26}$$

In (3.26), matching to the outer solution has been secured up to and including the terms of order $\epsilon^2 \ln\epsilon$. Matching the terms of order ϵ^2 requires consideration of $\phi(Y, \vartheta, \tau)$.

From (3.26), the leading term in the expansion of the critical layer vorticity is

$$\zeta = \phi_{YY} + \cdots. \tag{3.27}$$

Noting that $Z_C(r_2) = 0$, the leading-order terms from the vorticity equation (3.3) are

$$\phi_{YY\tau} + [\Omega_S(r_2) + Y\tilde{\Omega}_C'(r_2)]\phi_{\vartheta YY} - r_2^{-1}a_\vartheta\phi_{YYY} = r_2^{-1}Z_S'(r_2)a_\vartheta, \tag{3.28}$$

where $a(\vartheta, \tau) = \psi^0(r_2, \vartheta, \tau)$ is defined in (3.8).

When $|Y|$ is large, the dominant balance in (3.28) is between the right-hand side and the term proportional to Y on the left. Thus

$$\phi_{YY} \sim \frac{\mu_2 a}{Y} \quad \text{as } |Y| \to \infty. \tag{3.29}$$

The result above shows that ϕ_{YY} matches the second radial derivative of ψ_2^1 in (3.18).

The jump $c^+ - c^-$ is now obtained from the critical-layer expansion as

$$c^+ - c^- = \lim_{Y^\pm \to \pm\infty} \left[\int_{Y^-}^{Y^+} \oint \mathrm{e}^{-2\mathrm{i}\vartheta}\phi_{YY}\,\frac{\mathrm{d}\vartheta\mathrm{d}Y}{2\pi} - \mu_2\hat{a}\ln\left|\frac{Y^+}{Y^-}\right|\right]. \tag{3.30}$$

Here, $Y^\pm = (r^\pm - r_2)/\epsilon$ represent coordinates in the matching regions where $|r - r_c|$ becomes small (but not smaller than ϵ) and $|Y|$ becomes large (though not as large as $1/\epsilon$). But, in the asymptotic theory, we may further take the limit $\epsilon \to 0$, and then replace the limits of the integral in (3.30) by $\pm\infty$.

https://doi.org/10.1017/S0022112000002159 Published online by Cambridge University Press

3.5. *Summary and canonical form*

We now have a closed system of equations: the amplitude of the Kelvin mode, $\hat{a}(\tau)$, is determined by solving the ordinary differential equation (3.22). But the right-hand side of (3.22) involves the jump $c^+ - c^-$, which must be calculated by solving the critical-layer vorticity equation (3.28), and evaluating the principal part integral in (3.30). The radial advection in the critical-layer vorticity equation is due solely to the velocity field of the mode (these are the terms involving a_ϑ in (3.28)). The azimuthal advection in (3.28) results from the velocity of the main vortex, $\tilde{\Omega}_{\rm C}(r) + \epsilon\Omega_{\rm S}(r)$; this term appears as the Taylor-expanded form $\Omega_{\rm S}(r_2) + Y\tilde{\Omega}'_{\rm C}(r_2)$.

To remove distracting constants it is helpful to 'rescale' the final system. Because $\tilde{\Omega}'_C(r_2)$ is negative, the sign of μ_2 in (3.16) is opposite to that of $Z'_{\rm S}(r_2)$ and we define

$$\beta \equiv \mathrm{sgn}\,(\mu_2) = -\mathrm{sgn}\,(Z'_{\rm S}(r_2)). \tag{3.31}$$

If $\beta = -1$ the skirt has increasing vorticity as a function of r and consequently the Kelvin mode is destabilized. Although our main concern is the stable case, $\beta = +1$, for completeness we retain the parameter β as a 'switch' which distinguishes the two possibilities.

The constant μ_2 in (3.16) has the dimensions of inverse 'length' and $\mathscr{I}_1$ in (3.23) is positive with dimensions (time)/(length). The most compact final form is obtained by introducing the space and time scales,

$$\mathscr{L} \equiv -|\mu_2|/\mathscr{I}_1\tilde{\Omega}'_{\rm C}(r_2), \qquad \mathscr{T} \equiv \mathscr{I}_1/|\mu_2|. \tag{3.32}$$

These scales are used to define non-dimensional variables t, θ and y by

$$t \equiv \tau/\mathscr{T}, \quad \theta \equiv \vartheta - \varpi t/2, \quad y \equiv -\mathscr{L}^{-1}[(\Omega_{\rm S}/\tilde{\Omega}'_{\rm C}) + Y] - \varpi/2, \tag{3.33}$$

where $\varpi \equiv -\mathscr{T}(\mathscr{I}_2 + \mathscr{I}_3 + \mathscr{I}_4)/\mathscr{I}_1$. We are now recycling some notation by using (t, θ) for the non-dimensional time and angle in the equation above, and (ψ, ζ) for streamfunction and vorticity below. The context will imply our meaning. Finally, we define

$$\hat{\varphi}(t) \equiv (\mathscr{T}/r_2\mathscr{L})\hat{a}(\tau)e^{\mathrm{i}\varpi t}, \quad \zeta \equiv (\mathscr{T}/r_2|\mu_2|)\phi_{YY}, \quad \chi(t) \equiv (\mathscr{I}_5\mathscr{T}^2/\mathscr{I}_1 r_2\mathscr{L})\hat{b}(\tau)\exp(\mathrm{i}\varpi t). \tag{3.34}$$

With the definitions above the streamfunction is now

$$\psi \equiv -(y^2/2) + \varphi(\theta, t), \qquad \varphi(\theta, t) \equiv \hat{\varphi}(t)\mathrm{e}^{2\mathrm{i}\theta} + \hat{\varphi}^*(t)\mathrm{e}^{-2\mathrm{i}\theta}, \tag{3.35}$$

and the vorticity advection equation (3.28) is

$$\zeta_t + \frac{\partial(\psi, \zeta + \beta y)}{\partial(\theta, y)} = \zeta_t + y\zeta_\theta + \varphi_\theta\zeta_y + \beta\varphi_\theta = 0. \tag{3.36}$$

The evolution of $\hat{\varphi}(t)$ is then obtained from (3.22) and (3.30). In terms of non-dimensional variables, this is

$$\mathrm{i}\hat{\varphi}_t = \chi + \langle \mathrm{e}^{-2\mathrm{i}\theta}\zeta\rangle, \qquad \text{where } \langle\cdots\rangle \text{ is} \qquad \langle f\rangle \equiv \mathscr{P}\int \mathrm{d}y \oint \frac{\mathrm{d}\theta}{2\pi} f(\theta, y, t). \tag{3.37}$$

The principal value integral in (3.37) is necessary because $\zeta \propto y^{-1}$ as $|y| \to \infty$. However, henceforth we will omit the $\mathscr{P}$ decoration on the understanding that we take the principal values of all integrals to assure convergence.

It is remarkable that the system in canonical form contains no parameters, except

https://doi.org/10.1017/S0022112000002159 Published online by Cambridge University Press

Scaling	Transformation	New system
A	$\theta' = \theta + \delta,\ y' = y$ $\zeta' = \zeta,\ \hat{\varphi}' = \hat{\varphi}\exp(-2\mathrm{i}\delta),\ \varphi' = \varphi$	$\zeta'_t + y'\zeta'_{\theta'} + \varphi'_{\theta'}\zeta'_{y'} + \beta\varphi'_{\theta'} = 0$ $\mathrm{i}\hat{\varphi}'_t = \chi\exp(-2\mathrm{i}\delta) + \langle\zeta'\exp(-2\mathrm{i}\theta')\rangle$
B	$\theta' = \pi/2 - \theta,\ y' = -y$ $\zeta' = -\zeta,\ \hat{\varphi}' = -\hat{\varphi}^*,\ \varphi' = \varphi$	$\zeta'_t + y'\zeta'_{\theta'} + \varphi'_{\theta'}\zeta'_{y'} + \beta\varphi'_{\theta'} = 0$ $\mathrm{i}\hat{\varphi}'_t = \chi^* + \langle\zeta'\exp(-2\mathrm{i}\theta')\rangle$
C	$\theta' = -\theta,\ y' = -y$ $\zeta' = -\zeta,\ \hat{\varphi}' = \hat{\varphi}^*,\ \varphi' = \varphi$	$\zeta'_t + y'\zeta'_{\theta'} + \varphi'_{\theta'}\zeta'_{y'} + \beta\varphi'_{\theta'} = 0$ $\mathrm{i}\hat{\varphi}'_t = -\chi^* + \langle\zeta'\exp(-2\mathrm{i}\theta')\rangle$
D	$t' = \alpha_1^{-1}\alpha_2^{-1}t,\ \theta' = \alpha_2^{-1}\theta,\ y' = \alpha_1 y$ $\zeta' = \alpha_1\zeta,\ \hat{\varphi}' = \alpha_1^2\hat{\varphi},\ \varphi' = \alpha_1^2\varphi$	$\zeta'_t + y'\zeta'_\theta + \varphi'_{\theta'}\zeta'_{y'} + \beta\varphi'_{\theta'} = 0$ $\mathrm{i}\hat{\varphi}'_t = \alpha_1^3\alpha_2\chi + \alpha_1\alpha_2\langle\zeta'\exp(-2\mathrm{i}\alpha_2\theta')\rangle'$
E	$\theta' = \theta + \int_0^t u(t_1)\,\mathrm{d}t_1,\ y' = y + u$ $\hat{\varphi}' = \hat{\varphi}\exp[2\mathrm{i}\int_0^t u(t_1)\,\mathrm{d}t_t]$	$\zeta'_{t'} + y'\zeta'_{\theta'} + (\varphi'_{\theta'} - u_t)\zeta'_{y'} + \beta\varphi'_{\theta'} = 0$ $\mathrm{i}\hat{\varphi}'_t + 2u\hat{\varphi}' = \chi\exp[2\mathrm{i}\int_0^t u(t_1)\,\mathrm{d}t_1]$ $+\langle\zeta'\exp(-2\mathrm{i}\theta')\rangle'$

TABLE 1. Scaling transformations of the model system. In the table, we define $\varphi' = \hat{\varphi}'\exp(2\mathrm{i}\theta') + \text{c.c.}$ In cases D and E, $\langle\,\rangle' = \alpha_2/(2\pi)\oint \mathrm{d}\theta' \int \mathrm{d}y'$ and $u(t)$ is an arbitrary function of time. Note that C can be made from A and B.

for $\beta = \pm 1$ and those which occur in the specification of the external forcing, $\chi(t)$. With $\beta = -1$, the system is similar to reduced descriptions of hydrodynamic instabilities derived by Churilov & Shukhman (1987) and Goldstein & Leib (1988). In this article, we are concerned exclusively with the stable case $\beta = +1$ so that the forcing term, $\chi(t)$, is necessary to kick the vortex into action. Analogous models have been developed in plasma physics to describe electrostatic waves (Imamura *et al.* 1969; O'Neil *et al.* 1971; Tennyson, Meiss & Morrison 1994; del-Castillo-Negrete 1998).

In fact, (3.35)–(3.37) are not the most general equations characterizing such problems. Because the leading-order background vorticity, Z_C, has no gradient at the Kelvin wave's critical layer, there is a term missing from (3.36). The additional term has the form $\kappa\varphi_t$, where κ is a constant (see, for example, Goldstein & Hultgren 1988). Both this new term and $\beta\varphi_\theta$ are often ignored in the plasma literature.

4. Properties of the model

In sections to follow, we present solutions to our model system (3.35)–(3.37). However, before getting into these explicit details, we mention some general properties of the system.

4.1. *Transformations*

Our model system has a number of interesting scaling transformations listed in table 1. Under some circumstances, depending on χ, these transformations leave the equations unchanged and thus are symmetries. For example, transformation B is a symmetry if χ is real, and C is a symmetry if χ is imaginary. Scaling D is not a symmetry, but proves useful later. Transformation E is a change into a moving reference frame that rotates with angular velocity $u(t)$.

If the forcing function χ is a complex constant multiplying a real function of time, then transformation A can be used to make χ real. In this case, in (3.37), $\hat{\varphi}(t)$ is

https://doi.org/10.1017/S0022112000002159 Published online by Cambridge University Press

imaginary and $\langle \zeta \sin 2\theta \rangle = 0$. We may then let

$$\breve{\varphi} = \mathrm{i}\hat{\varphi} \tag{4.1}$$

(with $\breve{\varphi}$ real), to reflect this property, and so the governing equations can be written in the real form,

$$\zeta_t + y\zeta_\theta + 4\breve{\varphi}\cos 2\theta(\beta + \zeta_y) = 0 \quad \text{and} \quad \breve{\varphi}_t = \chi(t) + \langle \zeta \cos 2\theta \rangle. \tag{4.2}$$

4.2. *The structure of the vorticity as* $y \to \infty$

Now we turn to the structure of the vorticity $\zeta(\theta, y, t)$ when y is large. An appreciation of this structure is necessary when we enforce boundary conditions on the critical-layer solution. In anticipation of the linear solution in (5.5), we look for a $|y| \gg 1$ solution of the nonlinear problem (3.36) and (3.37) in the form

$$\zeta = \sum_{n=1}^{\infty} y^{-n}\zeta_n(\theta, \eta, t), \qquad \eta \equiv yt. \tag{4.3}$$

By substituting (4.3) into (3.36) and matching up powers of y^{-n} (considering η to be fixed), we find

$$\zeta_1 = -\beta\varphi + \zeta_{\mathrm{H}1}, \qquad \zeta_2 = -\tfrac{1}{4}\beta\varphi_{t\theta} + \zeta_{\mathrm{H}2}, \tag{4.4}$$

where $\zeta_{\mathrm{H}n}(\theta, \eta, t) = \zeta_{\mathrm{H}n}(\theta - yt)$ is a homogeneous solution of the operator $\partial_t + y\partial_\theta$. The necessity of these sheared contributions to ζ is illustrated by the linear solution in (5.5) below: $\zeta_{\mathrm{H}n}$ is picked to ensure that the $y \gg 1$ expansion of ζ satisfies initial conditions.

In the numerical solutions of § 6 we use forcing functions such as $\chi = t\exp(-t)$ that switch on smoothly at $t = 0$. In this case, $\varphi(\theta, 0) = \zeta(\theta, y, 0) = 0$ and $\zeta_{1\mathrm{H}} = \zeta_{2\mathrm{H}} = 0$.

4.3. *Conservation laws*

Because (3.36) is an advection equation for the total vorticity, $q \equiv \zeta + \beta y$ (the critical-layer concentration plus the background), there is an infinitude of Casimir invariants. That is,

$$\frac{\mathrm{d}}{\mathrm{d}t}\langle \mathscr{C}(\zeta + \beta y)\rangle = 0, \tag{4.5}$$

where $\mathscr{C}$ is any function for which the integrals in $\langle\,\rangle$ are convergent.

There are also more invariants which involve the second equation (3.37). Specifically,

$$\left.\begin{gathered} \frac{\mathrm{d}}{\mathrm{d}t}(|\hat{\varphi}|^2 - \tfrac{1}{2}\langle y\zeta\rangle) = -\mathrm{i}(\hat{\varphi}^*\chi - \hat{\varphi}\chi^*), \quad \frac{\mathrm{d}}{\mathrm{d}t}\langle \psi\zeta\rangle = \mathrm{i}\chi^*\langle \zeta \mathrm{e}^{2\mathrm{i}\theta}\rangle - \mathrm{i}\chi\langle \zeta \mathrm{e}^{-2\mathrm{i}\theta}\rangle, \\ \frac{\mathrm{d}}{\mathrm{d}t}(|\hat{\varphi}|^2 + \tfrac{1}{4}\beta\langle \zeta^2\rangle) = -\mathrm{i}(\hat{\varphi}^*\chi - \hat{\varphi}\chi^*), \end{gathered}\right\} \tag{4.6}$$

which correspond to conservation of momentum, energy and enstrophy. In (4.6), ψ is the streamfunction defined in (3.35). Notice that convergence at large y of the integrals in (4.6) is assured if we take the integrals in $\langle\,\rangle$ first over θ, and then over y: from (4.4) the θ-averaged vorticity decays like y^{-3} as $y \to \infty$. This is rapid enough to ensure convergence of $\langle y\zeta\rangle$ and $\langle \psi\zeta\rangle$ as principal value integrals.

https://doi.org/10.1017/S0022112000002159 Published online by Cambridge University Press

4.4. *The forcing function*

Once we take $\beta = +1$, the only control parameters in our system appear in the specification of the forcing function. We select two sample forcings:

$$\text{(i)} \quad \chi = A\chi_1 = \frac{1}{T^2} At \exp(-t^2/2T^2) \tag{4.7}$$

and

$$\text{(ii)} \quad \chi = A\chi_2 = \frac{1}{T^2} At \exp(-t/T), \tag{4.8}$$

where, in both cases, A is the amplitude and T is the duration. In the limit $T \to 0$, both functions amount to an instantaneous kick: $\chi(t) = A\delta(t)$. (Notice that the t here is the slow time. Thus $\delta(t)$ means an impulse that is intermediate between the fast vortex-turnover time and the much slower evolution of the critical layer.) Because these two choices for χ have the form of a real function of time multiplying a possibly complex constant, we may use scaling D of table 1 to transform the equations to a new set in which A is purely real. Hence, from now on, χ and A are taken to be real and therefore $\hat{\varphi}(t)$ is imaginary. We use the notation $\breve{\varphi} = \mathrm{i}\hat{\varphi}$ for the real amplitude of the streamfunction, as in (4.1).

5. The weakly forced limit: $A \ll 1$

We first consider low-amplitude solutions. Because the disturbance is externally excited, the amplitude is given by the strength of the forcing, and so we may construct solutions perturbatively by focusing on relatively small forcing amplitudes. To leading order, we derive the linear dynamics and uncover the analogue of Bassom & Gilbert's inviscid decay, and connect these peculiar damped 'modes' of the skirted vortex to the related non-decaying eigenmode of a compact vortex. Next, by retaining higher order in the forcing strength, we build disturbances of finite amplitude and show that these disturbances do not completely decay, but leave behind 'remnants' that can act as sources of secondary instability. As a result, we anticipate that disturbances do not always decay. This sets the stage for the discussion of the coming sections in which we study the evolution of more strongly disturbed vortices.

5.1. *The linear theory*

One virtue of the amplitude equations (3.36) and (3.37) is that the linear versions, namely

$$\zeta_t + y\zeta_\theta + \beta\varphi_\theta = 0, \qquad \mathrm{i}\hat{\varphi}_t = \chi + \langle \mathrm{e}^{-2\mathrm{i}\theta}\zeta \rangle, \tag{5.1a,b}$$

can be solved in closed form. If we confine attention to the dynamically active harmonic (that is, take $\zeta = \hat{\zeta}(y,t)\exp(2\mathrm{i}\theta) + \text{c.c.}$) and adopt zero initial conditions, it then follows from (5.1a) that

$$\hat{\zeta} = -2\mathrm{i}\beta \mathrm{e}^{-2\mathrm{i}yt} \int_0^t \mathrm{e}^{2\mathrm{i}ys}\hat{\varphi}(s)\,\mathrm{d}s \tag{5.2}$$

and hence

$$\langle \mathrm{e}^{-2\mathrm{i}\theta}\zeta \rangle = -2\mathrm{i}\beta \int_0^t \hat{\varphi}(s)\,\mathrm{d}s \int_{-\infty}^{\infty} \mathrm{e}^{-2\mathrm{i}y(t-s)}\,\mathrm{d}y = -\mathrm{i}\pi\beta\hat{\varphi}. \tag{5.3}$$

On substituting (5.3) into (5.1b), we obtain

$$\hat{\varphi}_t + \pi\beta\hat{\varphi} = -\mathrm{i}\chi. \tag{5.4}$$

Thus, the linear problem is reduced to solving a simple ordinary differential equation.

https://doi.org/10.1017/S0022112000002159 Published online by Cambridge University Press

If $\beta = -1$, then the homogeneous solution to (5.4) grow exponentially. In this instance, the vortex is unstable and the Kelvin wave of the compact vortex is modified by the skirt into an unstable mode. Then the full system is equivalent to a weakly nonlinear description of unstable inviscid vortices (and, as mentioned above, is similar to systems derived for fluid shear flows and ideal plasmas). A study of this case would lead us to explore the azimuthally structured states that appear without external forcing (cf. van Heijst *et al.* 1991; Kloosterziel & Carnevale 1998). However, our interest is in stable vortices with $\beta = 1$ and henceforth we shall focus exclusively on this case.

With $\beta = +1$, the homogeneous solution of (5.4), $\hat{\varphi} \propto \exp(-\pi t)$, provides the simplest example of hydrodynamic Landau damping. That is, the streamfunction decays exponentially while the accompanying vorticity is sheared out to ever smaller scales without decaying in amplitude. The exponential decay of $\hat{\varphi}$ results from spatial averaging (the $\langle\,\rangle$ in (5.1*a*)).

This curious behaviour is illustrated by impulsively exciting the vortex: $\chi = A\delta(t)$. In this case, the solution is

$$\hat{\varphi} = -\mathrm{i}A\mathrm{e}^{-\beta\pi t}, \qquad \zeta = \frac{2\pi + 4\mathrm{i}\beta y}{\pi^2 + 4y^2}[\mathrm{e}^{-\pi\beta t} - \mathrm{e}^{-2\mathrm{i}yt}]A\mathrm{e}^{2\mathrm{i}\theta} + \text{c.c.} \tag{5.5}$$

Thus the streamfunction decays exponentially, in the usual fashion of Landau damping. We should not be deceived, however, into thinking that this signifies the presence of a discrete, decaying mode. In fact, the vorticity is evidently not separable in y and t, and so (5.5) cannot be a linear eigenfunction. Instead, the vorticity always remains order one, but becomes increasingly sheared: $\zeta \sim \exp 2\mathrm{i}(\theta - yt)$ for large time. This is the reason why we refer to the disturbance on the non-compact vortex as a Kelvin quasi-mode.

It is important to appreciate that our matched asymptotics leads us to an equation that predicts exponential decay of the streamfunction. By contrast, Bassom & Gilbert's (1998) Gaussian vortices have streamfunctions that decay algebraically along the pathway to axisymmetrization. We explain this discrepancy by realizing that the algebraic decay is typical of sheared disturbances that wind up at the core of the vortex. That wind-up is missing from our model because the external forcing excites a pattern whose vorticity distribution rotates rigidly in the core. Instead, we only find a sheared disturbance inside the critical ring of the Kelvin quasi-mode. Nevertheless, as in the problem of localized disturbances to shear flow in channels (Balmforth, del-Castillo Negrete & Young 1997), there are terms that lie at higher order in our inner expansion that do, in fact, lead to a protracted algebraic decay at large times. In principle, these corrections cannot be neglected at large times and our asymptotic theory ultimately breaks down. This is illustrated by solutions of the linear initial-value problem for perturbed vortices presented by Schecter *et al.* (1999) and Schecter (1999).

Because Landau damping is so important to understanding the experimental results of Driscoll & Fine (1990), Cass (1998), Schecter *et al.* (1999) and Schecter (1999), we pause to exhibit the dimensional expression for the damping rate, γ:

$$\gamma \equiv \frac{\pi\epsilon}{\mathscr{T}} \equiv \frac{\pi|\epsilon Z_{\mathrm{S}}'(r_2)|}{r_2|\Omega_{\mathrm{C}}'(r_2)|\mathscr{I}_1}. \tag{5.6}$$

In view of the dependence of the growth rate on the vorticity gradient of the skirt, it is clear that the damping of the Kelvin quasi-mode becomes arbitrarily small as the vortex is made more compact. Essentially, this observation allows us to reconcile

https://doi.org/10.1017/S0022112000002159 Published online by Cambridge University Press

the apparent difference between truly compact vortices and smooth, almost compact vortices. Whereas the latter do not have true discrete modes, they have quasi-modes with very low damping rates. As a result, these modes can appear much like the true modes of compact vortices. Ultimately, however, the quasi-mode wraps up the residual vorticity gradient inside the critical layer and must decay. In practice, this may occur over a timescale that is too long to be relevant.

Though we have considered only inviscid vortices, it is relevant at this juncture to mention a property of the viscous problem. Specifically, with the introduction of viscosity the Landau damped quasi-modes can be transformed into true eigenmodes. (Balmforth 1998). Thus the Kelvin quasi-mode may become a real eigenmode when a small amount of viscosity is present.

5.2. *Nonlinear corrections*

Now consider perturbations of small, but finite, amplitude. Specifically, we take $\chi = A\chi_1(t)$ as in (4.7). In this case, the *real* governing equations are

$$\zeta_t + y\zeta_\theta + 4\breve{\varphi}\cos 2\theta(1+\zeta_y) = 0 \quad \text{and} \quad \breve{\varphi}_t = A\chi_1(t) + \langle \zeta \cos 2\theta \rangle. \tag{5.7}$$

We now look for an asymptotic solution of the form

$$\zeta = A\zeta_1(y,\theta,t) + A^2\zeta_2(y,\theta,t) + \cdots \quad \text{and} \quad \breve{\varphi} = A\breve{\varphi}_1(t) + A^2\breve{\varphi}_2(t) + \cdots. \tag{5.8}$$

To order A, we recover the linear system

$$\zeta_{1t} + y\zeta_{1\theta} + 4\breve{\varphi}_1\cos 2\theta = 0 \quad \text{and} \quad \breve{\varphi}_{1t} = \chi_1(t) + \langle \zeta_1 \cos 2\theta \rangle. \tag{5.9}$$

As described above, the solution is a Landau-damped disturbance; the streamfunction is

$$\breve{\varphi}_1 = \frac{\mathrm{e}^{-\pi t} - \mathrm{e}^{-t/T}}{(1-\pi T)^2} - \frac{t\,\mathrm{e}^{-t/T}}{T(1-\pi T)}. \tag{5.10}$$

The Landau-damped piece of this solution is that with the damping rate π; the other portions of the solution, with decay rates of $1/T$ arise from the structure of the forcing function. (Similar decay terms appear in the classical Landau damping problem as a result of the structure of the initial condition – see Balmforth *et al.* 1997.) Note how the Landau damping becomes less important than this other form of decay when T becomes larger than π^{-1}. Also, despite appearances, there is no singularity in (5.10) when $\pi T = 1$.

The vorticity perturbation ζ_1 has a more complicated form than the impulsively excited version in (5.5); we quote only the long-time result:

$$\zeta_1 \to \frac{4}{\sqrt{\pi^2 + 4y^2}(1+4y^2T^2)} \sin\left[2(\theta - yt) + \Psi\right], \tag{5.11}$$

where Ψ is a time-independent phase. This increasingly sheared perturbation is illustrated in figure 5.

At order A^2, we have the vorticity equation,

$$\zeta_{2t} + y\zeta_{2\theta} + 4\breve{\varphi}_2\cos 2\theta = -4\breve{\varphi}_1\zeta_{1y}\cos 2\theta. \tag{5.12}$$

There is no homogeneous solution to this linear equation for ζ_2 because of the initial conditions. But, through the right-hand inhomogeneous term, there are two particular solutions: a correction to the azimuthal mean, $\bar{\zeta}_2(y,t)$, and a harmonic, $\zeta_2^H(y,t) + \text{c.c.}$

https://doi.org/10.1017/S0022112000002159 Published online by Cambridge University Press

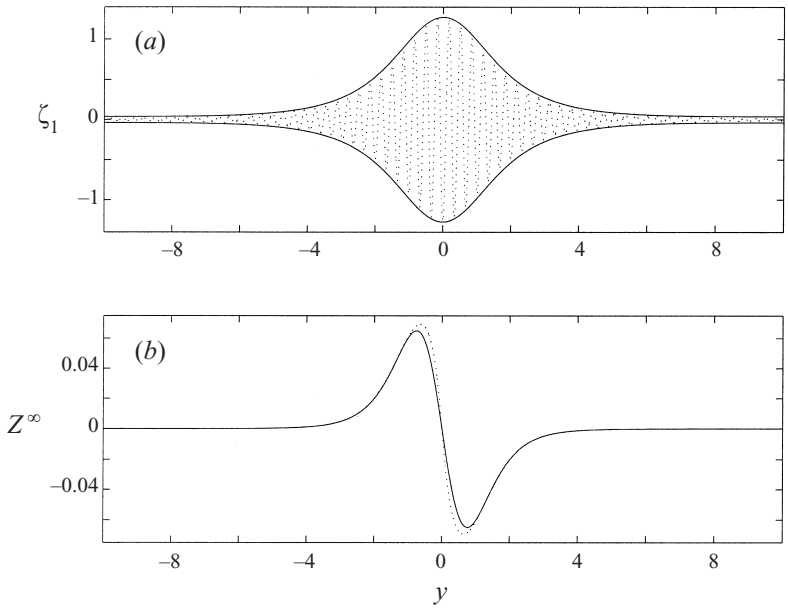


FIGURE 5. The vortical response of the quasi-mode to a low-amplitude disturbance, with $A = 0.5$ and $T = 0.2$. (*a*) The amplitude of the leading-order component of the vorticity of the quasi-mode for large times; the solid lines are the envelope of the prediction of the perturbation theory in (5.11) and the dotted curve shows the crenellating, $\exp 2\mathrm{i}\theta$, component of the vorticity in one of the numerical simulations of § 7 at $t = 10$. (*b*) The axisymmetrical remnant left behind by the perturbation, Z^∞. Again, the dotted line shows the remnant as determined from the numerical simulation.

Importantly, as $t \to \infty$,

$$\bar{\zeta}_2 \to Z^\infty = \partial_y \left[\frac{4}{(\pi^2 + 4y^2)(1 + 4y^2 T^2)^2} \right], \tag{5.13}$$

whereas the harmonic becomes increasingly sheared, just as the leading-order solution.

Thus, the externally excited disturbance does not completely decay away: besides the increasingly sheared quasi-mode, the disturbance leaves behind an axisymmetrical mean remnant, Z^∞. This remnant is also illustrated in figure 5. In other words, in a coarse-grained sense, the sheared, azimuthally structured part of the disturbance disappears over long times and the vortex axisymmetrizes. However, the azimuthal average is changed to order A^2.

5.3. *Secondary instabilities*

Although the remnant has no direct influence on the axisymmetrization of the vortex predicted by linear theory, there may be indirect effects arising from secondary instability. To see this, imagine that the disturbance has evolved towards the state described above, so that there is a mean axisymmetrical vorticity distribution inside the critical layer. Then, assume that the sheared, azimuthally structured part of the quasi-mode can be neglected because its coarse-grained average vanishes. This means we can treat the unperturbed state plus remnant as a new equilibrium vortex, and again perform a linear stability analysis.

The new stability equations are

$$\zeta_t + y\zeta_\theta + (1 + A^2 Z^\infty_y)\varphi_\theta = 0, \qquad \mathrm{i}\hat{\varphi}_t = \langle \mathrm{e}^{-2\mathrm{i}\theta}\zeta \rangle. \tag{5.14}$$

https://doi.org/10.1017/S0022112000002159 Published online by Cambridge University Press

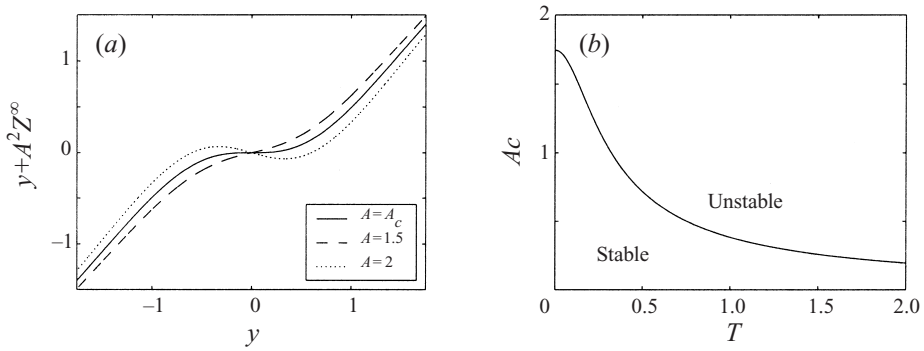


FIGURE 6. (*a*) New basic states for the secondary stability analysis with different values for A that straddle the critical case. (*b*) The critical amplitudes for onset of secondary instability, $A_c(T)$, as predicted by the perturbation theory.

Only the $m = 2$ azimuthal mode is relevant to stability, and so we set $\zeta = \hat{\zeta}(y)\exp(2\mathrm{i}\theta + \lambda t) + \text{c.c.}$ Then,

$$\hat{\zeta} = -\left(\frac{1 + A^2 Z_y^\infty}{y - \mathrm{i}\lambda/2}\right)\hat{\varphi}. \tag{5.15}$$

On substituting this solution into the equation for the streamfunction, we find

$$\lambda = -\pi\sigma + 8\mathrm{i}A^2 \int_{-\infty}^{\infty} \frac{\mathrm{d}y}{(\pi^2 + 4y^2)(1 + 4y^2T^2)^2(y - \mathrm{i}\lambda/2)^3}, \tag{5.16}$$

where $\sigma = \mathrm{sgn}(\lambda_r)$ and $\lambda = \lambda_r + \mathrm{i}\lambda_i$.

The integral in this dispersion relation can be performed analytically for arbitrary T. However it is convenient to first consider the case $T = 0$. Then, the relation can be rewritten in the form

$$(\lambda + \pi\sigma)^4 = 32A^2. \tag{5.17}$$

For $A \to 0$ we recover $\lambda = \lambda_r = -\pi\sigma$ and Landau damping. In the normal mode problem, the Landau-damped quasi-mode shows up as an inconsistent solution to the dispersion relation (5.17): one cannot satisfy the limiting equation when $\lambda_r/\sigma < 0$ because $\sigma \equiv \mathrm{sgn}(\lambda_r)$ (see also Balmforth *et al.* 1997).

The only consistent solution to (5.17) with positive σ is $\lambda = (32A^2)^{1/4} - \pi$, and exists provided that $(32A^2)^{1/4} > \pi$. An analogous solution exists for $\sigma < 0$. Thus, a direct instability ($\lambda_r > 0$ and $\lambda_i = 0$) occurs for

$$A > A_c = \frac{\pi^2}{4\sqrt{2}} \approx 1.745. \tag{5.18}$$

If $A < A_c$, there are no normal modes. One of the inconsistent solutions, however, again describes Landau damping, with a rate given by $\lambda_L = (32A^2)^{1/4} - \pi < 0$.

The critical amplitude, A_c, corresponds to a disturbance that generates a remnant for which the total vorticity of the new basic state, $y + A^2Z^\infty$, first develops extremal points: for $A > A_c$, $y + A^2Z^\infty$ is non-monotonic, as shown in figure 6(*a*). Möller & Montgomery (1999) have presented similar results in the context of the full equations of motion.

https://doi.org/10.1017/S0022112000002159 Published online by Cambridge University Press

When $T \neq 0$, the critical amplitude can again be determined:

$$A_c = \frac{\pi^2}{4\sqrt{2}} \frac{1}{\sqrt{1+2\pi^2 T^2}}. \tag{5.19}$$

This is shown in figure 6(b); as the turn-on time increases, the critical amplitude decreases.

To summarize, when we disturb the vortex, the induced perturbation does not completely decay away, but leaves a mean remnant that is itself unstable if the initial forcing amplitude is high enough. Thus, we cannot expect that the vortex always axisymmetrizes. In fact, if kicked hard enough, the vortex should suffer secondary instability and develop non-axisymmetrical structure; we explore this further in coming sections where we proceed to the opposite limit in which the forcing amplitude is relatively large, and then with numerical experiments on the full system.

Lastly, we note that even when the forcing amplitude is sub-threshold, $A < A_c$, the remnant still plays an important role. The Landau damping rate in the absence of the remnant is always π, but when the perturbation creates this extra mean vorticity, the Landau damping is modified and the rate of decay becomes $\lambda_L = (32A^2)^{1/4} - \pi$. Notably, the remnant reduces the Landau damping. This suggests that after an initial period of true Landau damping, the amplitude of the streamfunction should decay less quickly. We confirm this trend in the numerical results reported in § 7.

6. The strongly forced limit: $A \gg 1$

In the previous section we analysed the weakly forced limit in which A is small. In this section we turn to the complementary case in which A is large. Specifically, we consider the impulsive case by taking $T \to 0$ in (4.7) and (4.8) so that $\chi(t) = A\delta(t)$. We introduce a small parameter δ defined by

$$\delta \equiv \frac{1}{\sqrt{2A}}. \tag{6.1}$$

In the limit $\delta \to 0$ the dynamics can be reduced to a passive scalar advection problem. Notice that in order not to violate our original scaling assumptions, A cannot be as large as ϵ^{-1}. Consequently δ must be greater than $\sqrt{\epsilon}$.

6.1. *Reduction to a passive scalar problem*

By using scaling D of table 1 we make the following definitions: $\alpha_1 = \delta$ and $\alpha_2 = 1$; $t' = t/\delta$, $y' = \delta y$, $\zeta' = \delta\zeta$, $\hat{\varphi}' = \delta^2\hat{\varphi}$ and $\varphi' = \delta^2\varphi$. Notice that the forcing is $\chi = \delta(t)/2\delta^2 = \delta(t')/2\delta^3$. Dropping the primes, and introducing $\breve{\varphi} = \mathrm{i}\hat{\varphi}$, the rescaled equations are

$$\zeta_t + y\zeta_\theta + \zeta_y\varphi_\theta + \varphi_\theta = 0, \qquad \breve{\varphi}_t = \tfrac{1}{2}\delta(t) + \delta\langle\cos 2\theta\,\zeta\rangle. \tag{6.2}$$

We see that if $\delta \ll 1$ then the effect of the vorticity on the streamfunction is small and so we can solve (6.2) with a perturbation expansion of the form

$$\breve{\varphi} = \tfrac{1}{2} + \delta\breve{\varphi}_1 + \cdots, \qquad \zeta = \zeta_0 + \delta\zeta_1 + \cdots. \tag{6.3}$$

The leading-order vorticity, $q \equiv y + \zeta_0$, is obtained by solving a passive scalar advection equation:

$$q_t + yq_\theta + 2q_y\cos 2\theta = 0. \tag{6.4}$$

This passive scalar problem is discussed by O'Neil (1965), Stewartson (1978), Warn & Warn (1978) and Killworth & McIntyre (1985) in related contexts.

https://doi.org/10.1017/S0022112000002159 Published online by Cambridge University Press

The crucial point is that in this strongly forced limit, the leading-order streamfunction does not decay: $\breve{\varphi} = 1/2$ when $t > 0$. This behaviour is very different from the exponential decay in the weakly forced limit of the previous section. But $\breve{\varphi} = 1/2$ is only the leading-order term; to show that the strongly forced case does not relax back to axisymmetry we must obtain the next term in the expansion of $\breve{\varphi}$ and show that this correction, $\breve{\varphi}_1(t)$, is bounded as $t \to \infty$. The correction $\breve{\varphi}_1$ is obtained by first solving (6.4) and then calculating

$$\breve{\varphi}_1(t) = \int_0^t \langle \cos 2\theta\, \zeta_0(\theta, y, t') \rangle \, \mathrm{d}t' = \tfrac{1}{2} \big\langle y \zeta_0(\theta, y, t) \big\rangle \,. \tag{6.5}$$

This expression shows that $\breve{\varphi}_1(t)$ is bounded. We find below that as $t \to \infty$ the expression above gives $\breve{\varphi}_1(t) \to -1.543$.

To summarize, the following perturbative calculation shows that as $t \to \infty$ the streamfunction is $\breve{\varphi}(\infty) = (1/2) - 1.543\delta + O(\delta^2)$. This shows that nonlinearity prevents a perturbed vortex from relaxing back to axisymmetry.

6.2. *Details of the leading-order vorticity evolution*

We solve equation (6.4) by the method of characteristics (O'Neil 1965; Stewartson 1978). To make an analogy with the orbits of the pendulum we introduce $\xi = \theta - \pi/4$ so that the streamfunction is

$$\psi = -y^2/2 + \sin 2\theta = -y^2/2 + \cos 2\xi. \tag{6.6}$$

The Lagrangian orbits are obtained by solving the Hamiltonian system

$$\dot{\xi} = y, \qquad \dot{y} = -2 \sin 2\xi. \tag{6.7}$$

The streamfunction ψ is a constant of the motion and it is convenient to introduce

$$m \equiv \frac{2}{1 - \psi} = \frac{4}{y^2 + 4 \sin^2 \xi}. \tag{6.8}$$

The solution of (6.7) can then be given in terms of Jacobi elliptic functions (Abramowitz & Stegun 1972) as

$$\sin \xi = \operatorname{sn}(2t/\sqrt{m} + u_0; m), \qquad y = \frac{2}{\sqrt{m}} \operatorname{dn}(2t/\sqrt{m} + u_0; m). \tag{6.9a,b}$$

These expressions hold for $y > 0$. The solution for $y < 0$ may be obtained by inserting a minus sign in front of the dn. From now on, only $y > 0$ is considered. The constants of integration, u_0 and m, are determined by the initial condition (ξ_0, y_0):

$$\sin \xi_0 = \operatorname{sn}(u_0; m) \quad \text{and} \quad y_0 = \frac{2}{\sqrt{m}} \operatorname{dn}(u_0; m). \tag{6.10}$$

At time t, (6.9) and (6.10) define a mapping between the current point (ξ, y, t) and the initial point $(\xi_0, y_0, 0)$ of the Lagrangian trajectory.

To obtain the vorticity $q(\xi, y, t)$, we must determine the initial position (ξ_0, y_0) as a function of the current position (ξ, y). Then, because q is constant along a trajectory, and because $q(\xi, y, 0) = y$, the solution of (6.4) is simply

$$q(\xi, y, t) = y_0 = \frac{2}{\sqrt{m}} \operatorname{dn}(u_0; m). \tag{6.11}$$

In (6.8) we already have $m(\xi, y)$ to hand. The chore is to determine $u_0(\xi, y, t)$ by solving (6.9). There are two special cases in which $u_0(\xi, y, t)$ is easily obtained so

https://doi.org/10.1017/S0022112000002159 Published online by Cambridge University Press

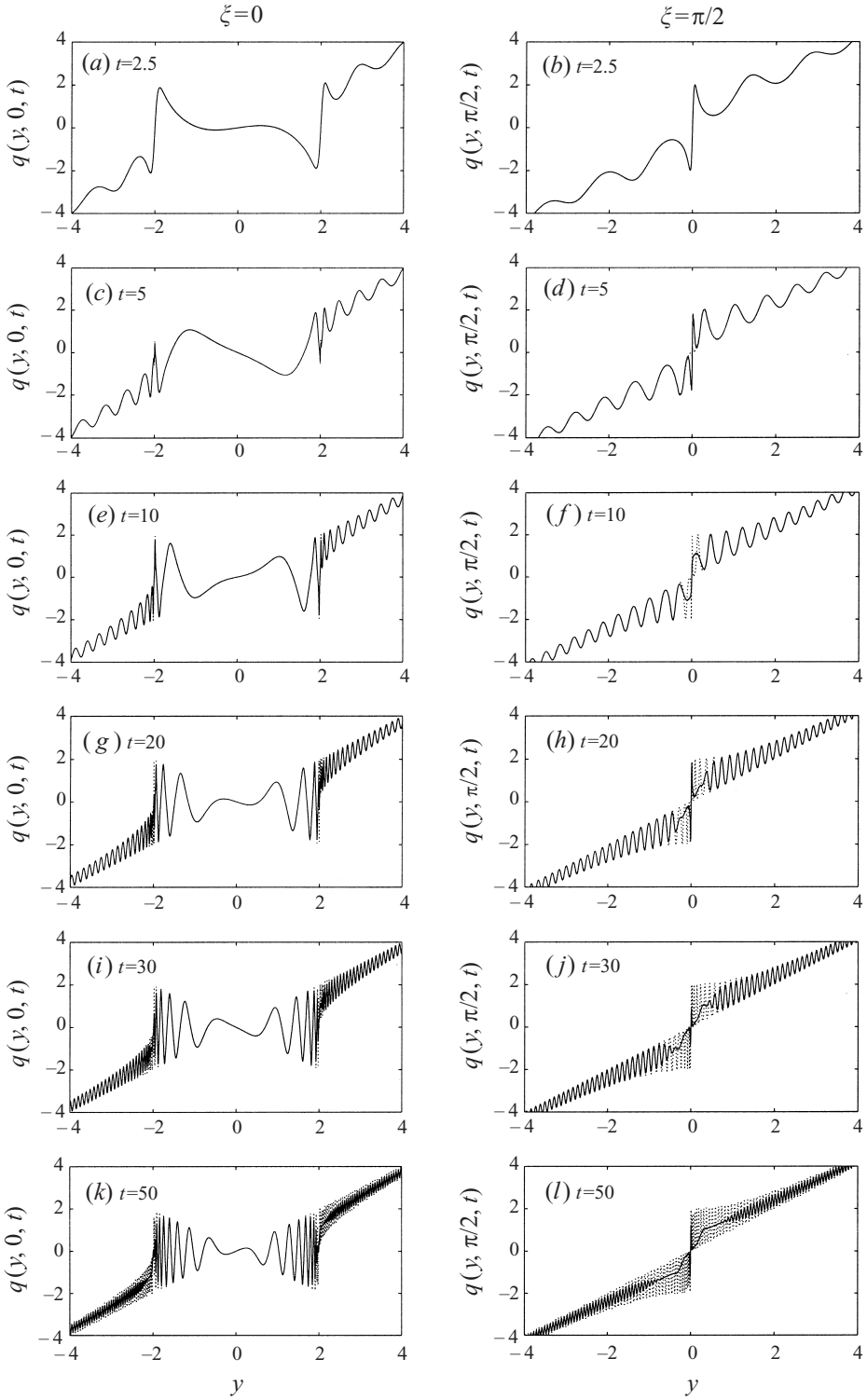


FIGURE 7. A comparison of the numerical solution (solid) of the passive scalar equation (6.4) with the exact solution (dotted) along $\xi = 0$ and $\xi = \pi/2$ (or $\theta = \pi/4$ and $\theta = 3\pi/4$). Shown is the total leading-order vorticity, $q = y + \zeta$, at the times indicated. At $t = 50$ the centre of the cat's eye has turned over almost 16 times.

https://doi.org/10.1017/S0022112000002159 Published online by Cambridge University Press

that explicit solutions can be presented. These two cases correspond to determining $q(\xi, y, t)$ along the lines $\xi = 0$ and $\xi = \pi/2$ (equivalently $\theta = \pi/4$ and $3\pi/4$).

For $\xi = 0$, we have $m = 4/y^2$ and so from (6.9*a*), $u_0 = -2t/\sqrt{m}$. Hence,

$$q(\xi = 0, y, t) = y\ \mathrm{dn}(yt; 4/y^2). \tag{6.12}$$

This solution is a vertical slice bisecting the pupil of the cat's eye. Similarly, along the line $\xi = \pi/2$, we have $m = 4/(4 + y^2)$. Then from (6.9*a*) $u_0 = \mathrm{K}(m) - 2t/\sqrt{m}$ where $\mathrm{K}(m)$ is a complete elliptical integral of the first kind. On this second slice,

$$q(\xi = \pi/2, y, t) = \frac{2}{\sqrt{m}}\ \mathrm{dn}\left[\mathrm{K}(m) - \frac{2t}{\sqrt{2m}}; m\right], \qquad m = \frac{4}{4 + y^2}. \tag{6.13}$$

This slice passes through the hyperbolic point (the corner of the cat's eye).

The solutions above are illustrated in figure 7. This figure compares the elliptic-function solutions above to those obtained by numerically integrating equation (6.4) using the method of Appendix A. Evident is an increasingly violent crenellation of the vorticity distribution, which is essentially the same process that operates in the linear problem to produce Landau damping. As the oscillation become increasingly fine, eventually the numerical procedure is inaccurate; in figure 7 this failure is first evident at $\xi = \pi/2$ and $t = 10$. Also in figure 7, a significant departure from linear theory is that the vorticity now turns over completely within the cat's eye. This is illustrated more fully in figure 8.

6.3. *The first-order correction to the streamfunction*

With $q = y + \zeta_0$ to hand, we can obtain the first-order correction to the streamfunction, $\breve{\varphi}_1(t)$ in (6.5). The calculation, which largely follows O'Neil (1965), is in Appendix B and the result is

$$\breve{\varphi}_1(t) = -16\pi \int_0^\infty \frac{\mathrm{d}m}{m^{5/2}\mathrm{K}(m)} \sum_{N=1}^{\infty} \frac{\varpi^N}{(1 + \varpi^N)^2} [1 + \sigma(-1)^N] \left\{1 - \cos\left[\frac{\pi N t}{\sqrt{m}\mathrm{K}(m)}\right]\right\}, \tag{6.14}$$

where

$$\varpi(m) \equiv \exp\left[-\frac{m\mathrm{K}(1-m)}{\mathrm{K}(m)}\right], \qquad \sigma(m) = \begin{cases} 1 & \text{if } m < 1, \\ -1 & \text{if } m > 1. \end{cases} \tag{6.15}$$

The function $\breve{\varphi}(t)$ is shown in figure 9; as remarked earlier, the correction decays, with oscillations, to a constant level.

6.4. *The final coarse-grained state*

The solutions above indicate that as $t \to \infty$ the vorticity becomes crenellated in y. The amplitude of these wiggles remains finite but their scale is increasingly fine as $t \to \infty$. A coarse-grained average filters the oscillations and reveals a non-trivial structured averaged field (see figure 10*a*). Because of symmetry this averaged vorticity is zero within the cat's eye (that is, within the area where $\psi > -1$). Outside the cat's eye, the averaged vorticity takes a non-zero mean value, which we now calculate.

We determine that coarse-grain average by arguing that advection cannot transfer any vorticity through the steady streamlines and consequently the amount of vorticity contained within the differential area enclosed by two adjacent streamlines (a streamtube) is constant. Thus the coarse-grained average is obtained by taking the initial vorticity pattern, $q(\xi, y, 0) = y$, and making an average over a streamtube. Following

https://doi.org/10.1017/S0022112000002159 Published online by Cambridge University Press

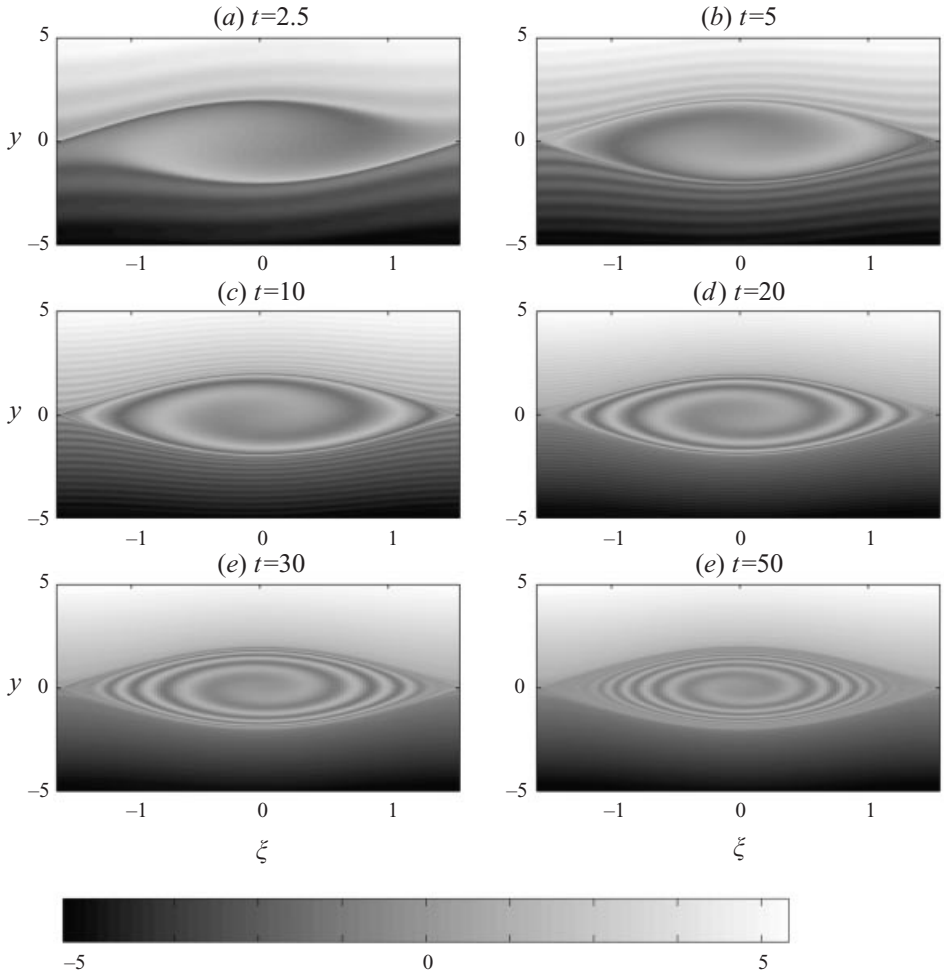


FIGURE 8. A numerical solution of the passive scalar equation (6.4). Shown is a grey-scale map of the total leading-order vorticity, $q = y + \zeta$, at the times indicated.

Rhines & Young (1983), this streamtube average is

$$\bar{q}(\psi) = \oint y \frac{\mathrm{d}\ell_\psi}{|\nabla\psi|} \Big/ \oint \frac{\mathrm{d}\ell_\psi}{|\nabla\psi|}, \tag{6.16}$$

where ℓ_ψ is the arclength around a streamline. It is clear from the symmetry of the initial condition that $\bar{q}(\psi) = 0$ within the region of closed streamlines where $\psi > -1$.

Outside the cat's eye, where $\psi < -1$, the streamtube average is non-zero, and can be calculated by converting the contour integrals in (6.16) to integrals with respect to ξ. This calculation is given in the related context of a forced critical layer by Killworth & McIntyre (1985). From Appendix A of Killworth & McIntyre, we quote the result:

$$\bar{q}(\psi) = \pm 2\pi \left[\int_{-\pi}^{\pi} \frac{\mathrm{d}\xi}{\sqrt{2(\cos 2\xi - \psi)}} \right]^{-1} = \pm \frac{\pi}{\sqrt{m}\mathrm{K}(m)}, \tag{6.17}$$

https://doi.org/10.1017/S0022112000002159 Published online by Cambridge University Press

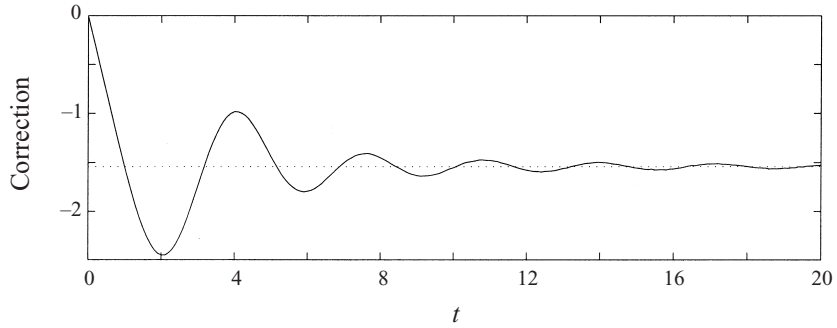


FIGURE 9. The function $\breve{\varphi}_1(t)$. The asymptotic behaviour is given by $\breve{\varphi}_1(t) \to -1.543$, shown by the dotted line.

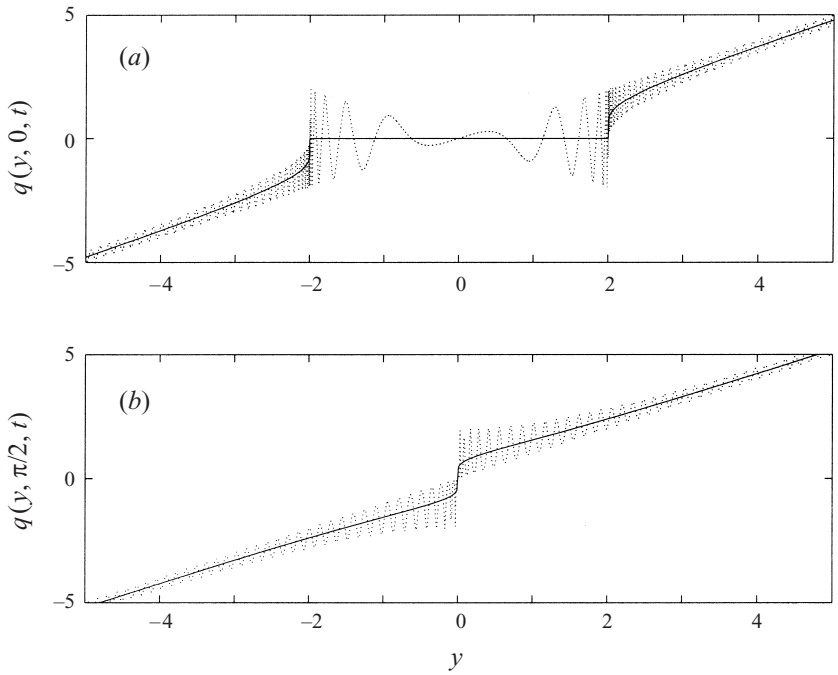


FIGURE 10. Exact solutions and coarse-grained averages along (*a*) $\xi = 0$ ($\theta = -\pi/4$) and (*b*) $\xi = \pi/2$ ($\theta = \pi/4$), at $t = 25$. The dotted lines show the solution; the solid line is the coarse-grain final state calculated from (6.17).

where the sign is chosen to ensure that $\bar{q}(\psi)$ is an odd function of y with the same sign as y. This average vorticity distribution is shown as the solid curve in figure 10.

Figure 9 shows that as $t \to \infty$ the streamfunction correction $\breve{\varphi}_1(t)$ approaches a constant. The constant $\breve{\varphi}_1(\infty)$ can be computed directly from (6.3) by neglecting the time-dependent term (which oscillates in m with finer and finer scale as time proceeds, reflecting phase mixing inside and outside the cat's eyes) and using some elliptic function relations (see O'Neil 1965). The constant can also be calculated by inserting the coarse-grained vorticity distribution, $\bar{q}(\psi)$ in (6.17), to evaluate the second integral in (6.5). This calculation is also in Appendix A of Killworth & McIntyre. We quote the result that $\breve{\varphi}_1(\infty) \approx -1.543$.

https://doi.org/10.1017/S0022112000002159 Published online by Cambridge University Press

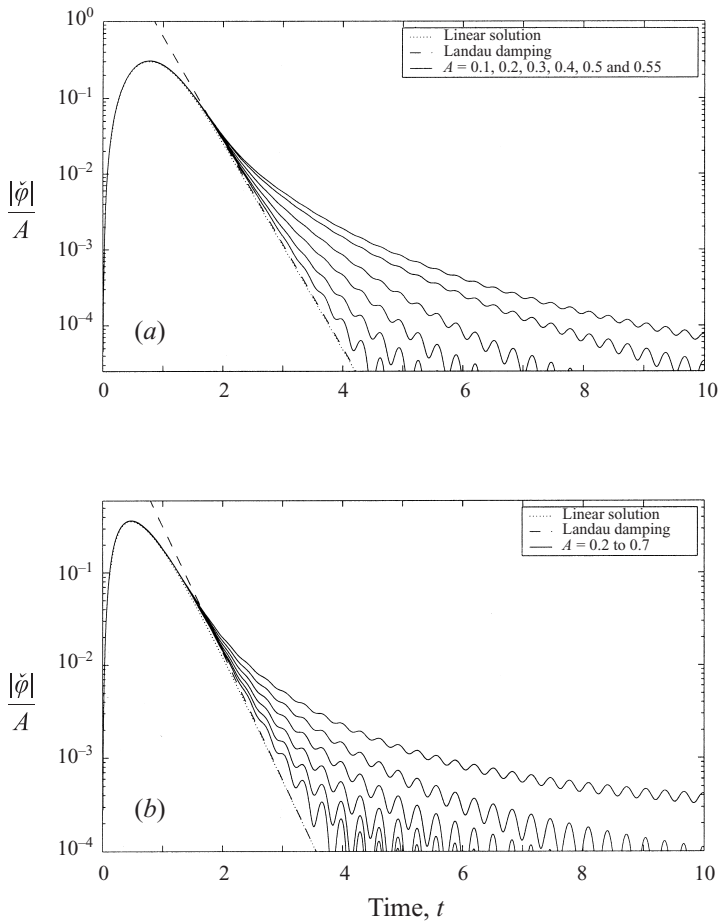


FIGURE 11. Scaled streamfunction amplitudes, $|\check{\varphi}(t)|/A$, against time for (*a*) $\chi = A\chi_1$ and $T = 0.5$, and (*b*) $\chi = A\chi_2$ and $T = 0.2$. In each case, results for different forcing amplitudes, A, are shown, The linear result is also shown together with the trend of Landau damping.

7. Numerical integrations

We now turn to the full nonlinear problem for arbitrary forcing and solve the equations numerically. The integration scheme is described in Appendix A; it is an operator splitting scheme based on the algorithm of Cheng & Knorr (1976). We use the two forcing functions in (4.7) and (4.8). The first of these is characterized by a disturbance that always, eventually, subsides in comparison to the Landau damping. The second, however, decays less quickly than the Landau damping if $T > \pi^{-1}$. The goal of the computations is to make contact with the preceding analytic arguments and study the formation of cat's eyes. Specifically, we delineate the regions of the (A, T)-plane within which axisymmetrization occurs.

7.1. *Weak forcing*

We first present results of simulations for low-amplitude forcings. By 'low-amplitude', here, we mean simulations that appeared to show axisymmetrization ($\check{\varphi} \to 0$ as $t \to \infty$). As indicated above, such behaviour can only be expected for values of the forcing amplitude A below some threshold depending on T.

https://doi.org/10.1017/S0022112000002159 Published online by Cambridge University Press

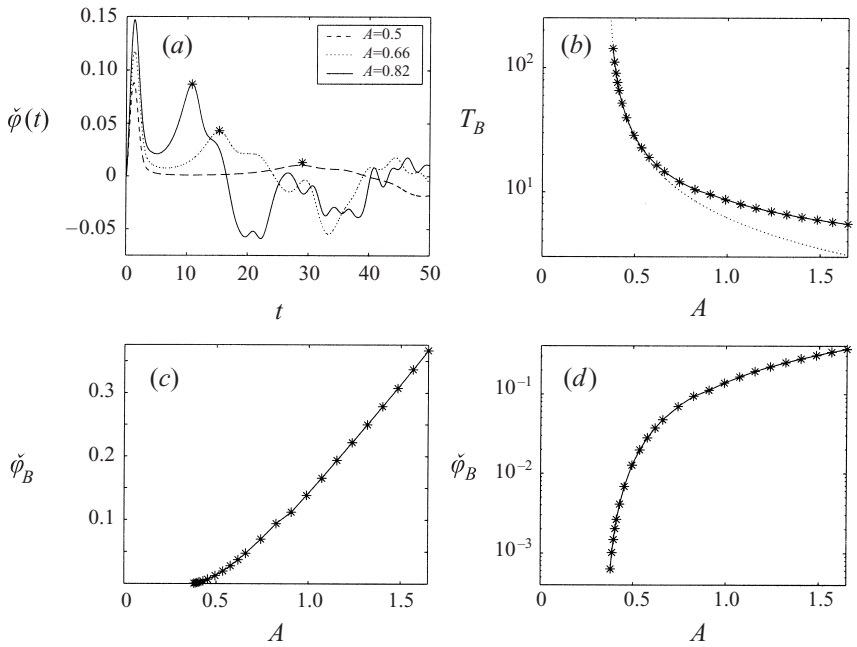


FIGURE 12. The definition of the first bounce time, T_B, and amplitude, $\breve{\varphi}_B = \breve{\varphi}(T_B)$, are illustrated in (*a*), for three cases using the forcing function $\chi = A\chi_1$ with $T = 1$. The stars show the points $(T_B, \breve{\varphi}_B)$. (*c*)–(*d*) These quantities against A. (*b*) We also add the curve, $T_B = 4.02/(A - 0.3525)$ which tolerably fits the apparent divergence of the bounce time near $A = 0.35$.

In figure 11 we show streamfunction amplitude as a function of time for both $\chi = A\chi_1$ and $\chi = A\chi_2$. The solutions all show an initial evolution that follows the linear theory. But beyond a certain time, the Landau damping is interrupted by a slower decay. We interpret this slow decay to be the effect of the remnant, Z^∞, described in § 5.3. Note that the low-amplitude oscillations in figure 11 that become visible at about $t = 4$ arise due to the finite domain in which the system is numerically solved (see Appendix A). These are spurious, as can be seen by changing the domain size which changes their amplitude and period.

As predicted by the asymptotic theories of § 4, the streamfunction decays provided $A < A_c(T)$; that is, the vortex axisymmetrizes. If $A > A_c(T)$, the streamfunction enters a different behavioural regime in which φ undergoes large-amplitude oscillations (see figure 12*a*). These 'bounces' coincide with the initial turning over of a cat's eye, as explored in more detail shortly.

A physical rationale for the threshold is that there are two characteristic timescales in the problem (excluding T, which complicates the argument): the time for Landau damping and the characteristic turnover time in the core of the cat's eye. Now, broadly speaking, if the damping time greatly exceeds the turnover time, we may expect that cat's eyes form without much decay of the streamfunction. However, if the damping time is much shorter than the turnover time, a cat's eye cannot complete even one bounce before it disappears. Hence, there should be an amplitude threshold if the two effects are competitive.

To estimate the threshold, we measure the time and amplitude of the first 'bounce' after the initial excitation of the quasi-mode, T_B and $\breve{\varphi}_B = \breve{\varphi}(T_B)$ respectively. This is illustrated in figure 12. In this figure we also display the dependence of T_B and $\breve{\varphi}_B$

https://doi.org/10.1017/S0022112000002159 Published online by Cambridge University Press

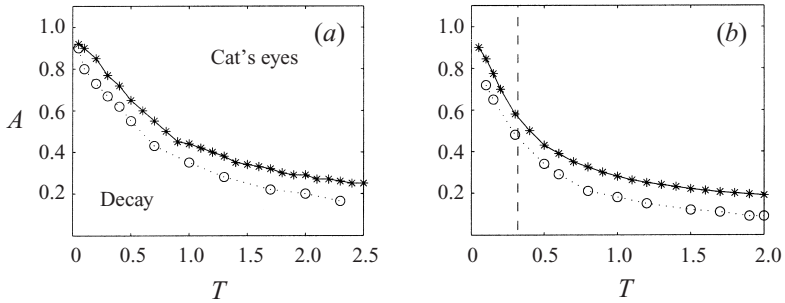


FIGURE 13. Forcing amplitudes, A, as functions of T for simulations in which T_B first exceeded about 45 time units. (*a*) The Gaussian case, $\chi = A\chi_1$, and (*b*) the exponential, $\chi = A\chi_2$. The vertical dashed line in (*b*) shows the turn-on time for which $\pi T = 1$ (for the significance of this, see (5.10) and the subsequent discussion). These curves are upper bounds on the critical amplitudes below which cat's eyes ultimately do not form. More detailed computations show that the threshold may be somewhat below this upper bound; the circles indicate a selection of better estimates computed by extrapolation using fits like that shown in figure 12.

upon A for the Gaussian forcing function. These data present the evidence that as A tends to a critical value from above, $T_B \to \infty$, and the streamfunction decays for lower A.

The critical values of the amplitude A for which bouncing ensues are plotted against T in figure 13 for both χ_1 and χ_2. These amplitudes are estimated by determining when T_B first exceeds 45 time units as we lower A. This places an upper limit on $A_c(T)$ and avoids numerical errors that can accumulate in long time integrations with low-amplitude streamfunctions. The figure also shows extrapolated estimates of the threshold using fits like that shown in figure 12(*b*). Despite this evidence for a cut-off, we cannot say definitively whether disturbances excited by forcing amplitudes below this curve always ultimately decay, or whether the bounce time merely becomes longer and longer. But all evidence from our simulations suggests that if $A < A_c$ the streamfunction decays.

7.2. *Formation of cat's eyes*

When $A > A_c$, we unambiguously observe the creation of cat's eye structures. A typical example is shown in figure 14 for $\chi = A\chi_2$ with $T = 1$. Qualitatively, the visual appearance of the cat's eyes is not sensitive to A and T, nor to the type of forcing function, provided A significantly exceeds the critical threshold. This remains true even when the forcing function decays less quickly than the natural Landau damping.

We compare runs with different values of A in figures 15–17. The solutions in panels (*a*) and (*b*) of these figures have smaller values of A and the streamfunction amplitudes follow the linear solution over relatively long initial times. However, the third solution in panel (*c*) departs from the linear case almost immediately. In each case, the decay of the streamfunction halts and $\hat{\varphi}(t)$ begins to oscillate. The inception of these oscillations corresponds to the initiation of circulation in the core of the cat's eye.

There are two main differences between cases with low and high A. The first is that the crenellation of ζ is far more significant in lower-amplitude solutions (see figures 16 and 17). The result is that the cat's eye has a more complicated structure in its early stages of development (and is consequently more prone to numerical error).

The second difference concerns the streamfunction. For small A, $\check{\varphi}(t)$ passes repeatedly through zero (see figures 15*a*, *b* and 12*a*). This means that the vortex core

https://doi.org/10.1017/S0022112000002159 Published online by Cambridge University Press

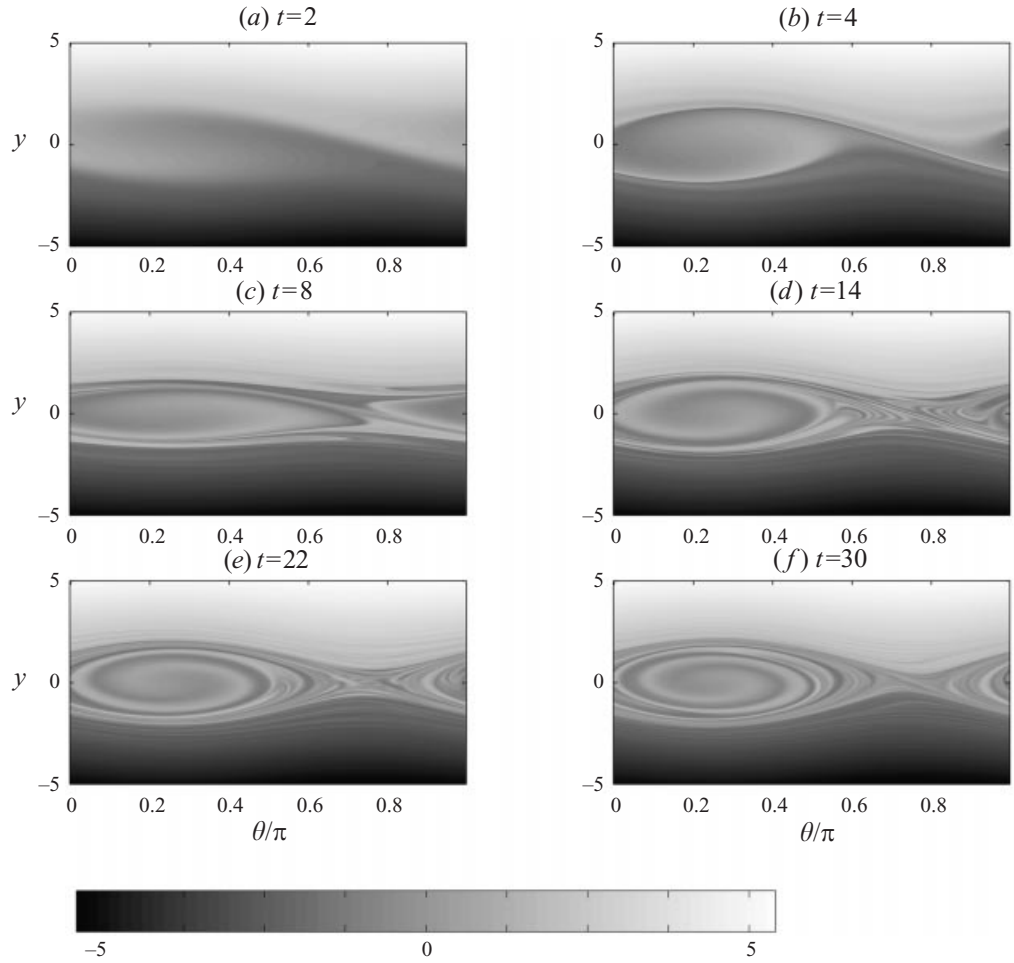


FIGURE 14. A solution with $\chi = 2.72\chi_2$ with $T = 1$. Shown is a grey-scale map of the total vorticity, $y + \zeta$, at the times indicated.

overturns one way for a while, but then unwinds for a subsequent interval. Overall, it is not clear whether the core ultimately creates a cat's eye, or whether the vorticity simply continues to wind and unwind. In other words, the asymptotic state may be time dependent (and reminiscent of solutions described by Warn & Gauthier 1989, in a loosely related problem). For large A, the streamfunction remains of one sign: $\breve{\varphi}(t)$ rises to some value, and then oscillates about that level. There is some suggestion that the oscillations decay with time, perhaps reflecting phase mixing within the cat's eye (as in O'Neil's solution), and that there is a slight drift in the overall level of $\breve{\varphi}(t)$ (see figure 15*c*, and also 18*d*). This slow drift is caused by numerical smoothing (see Appendix A).

7.3. *Coarse-grained steady states*

Both the numerical results and the strongly forced problem illustrate the importance of finite-amplitude steady states. These states are described by the time-independent version of our model system, which implies that $q = y + \zeta$ is any function of the total streamfunction, $\psi = -y^2/2 + 2\breve{\varphi}\cos 2\theta$. That is, $\zeta + y = q(\psi)$. This function need only

https://doi.org/10.1017/S0022112000002159 Published online by Cambridge University Press

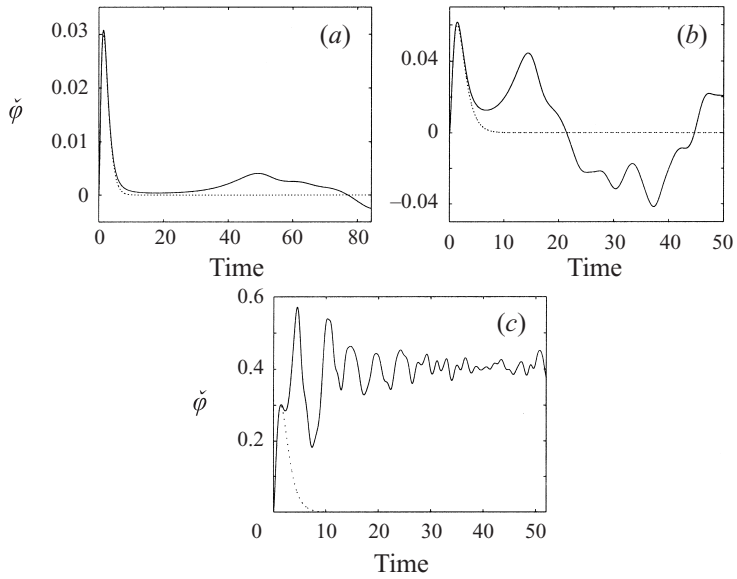


FIGURE 15. Streamfunction evolution for (*a*) $\chi = 0.272\chi_2$, (*b*) $\chi = 0.544\chi_2$, and (*c*) $\chi = 2.72\chi_2$, with $T = 1$. In this case, $\hat{\varphi}$ is purely imaginary and the linear solution is also shown by dotted lines.

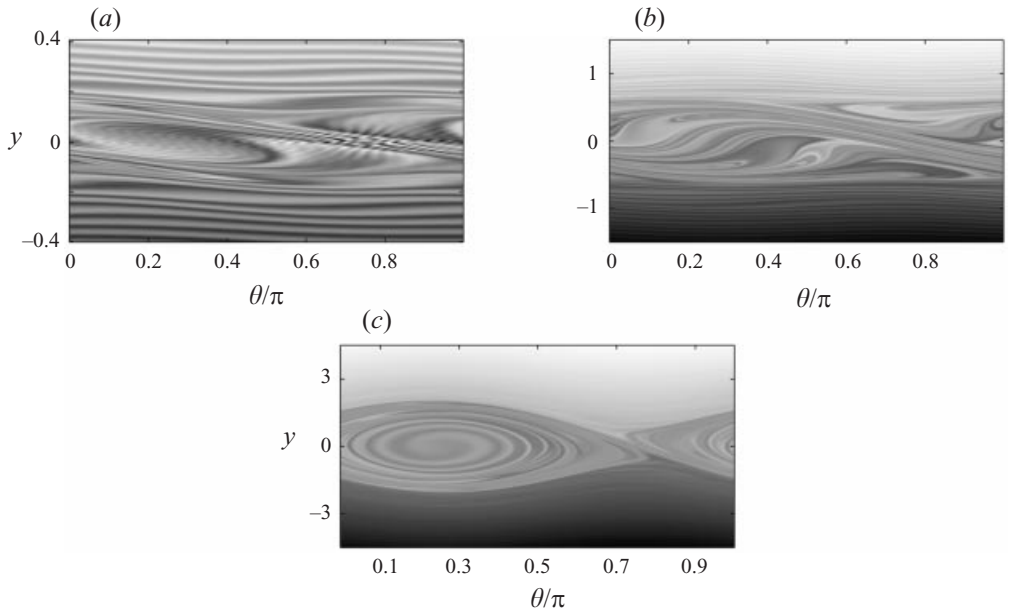


FIGURE 16. Grey-scale pictures of constant total vorticity $y + \zeta$ for (*a*) $\chi = 0.272\chi_2$, (*b*) $\chi = 0.544\chi_2$, and (*c*) $\chi = 2.72\chi_2$, with $T = 1$. These snapshots are taken at $t = 90$ for (*a*), and $t = 60$ for (*b*) and (*c*). Note that the vertical scale changes in each panel, and the entire domain is not shown.

satisfy the consistency condition, $\langle e^{-2i\theta} q(\psi) \rangle = 0$, which does not greatly constrain the possibilities.

The initial condition used in the computations has $\psi = -q^2/2$. This relation is rapidly lost in the initial evolution. But over long times, there is evidence that the numerical solutions converge to states with another q, ψ relation. This is illustrated

https://doi.org/10.1017/S0022112000002159 Published online by Cambridge University Press

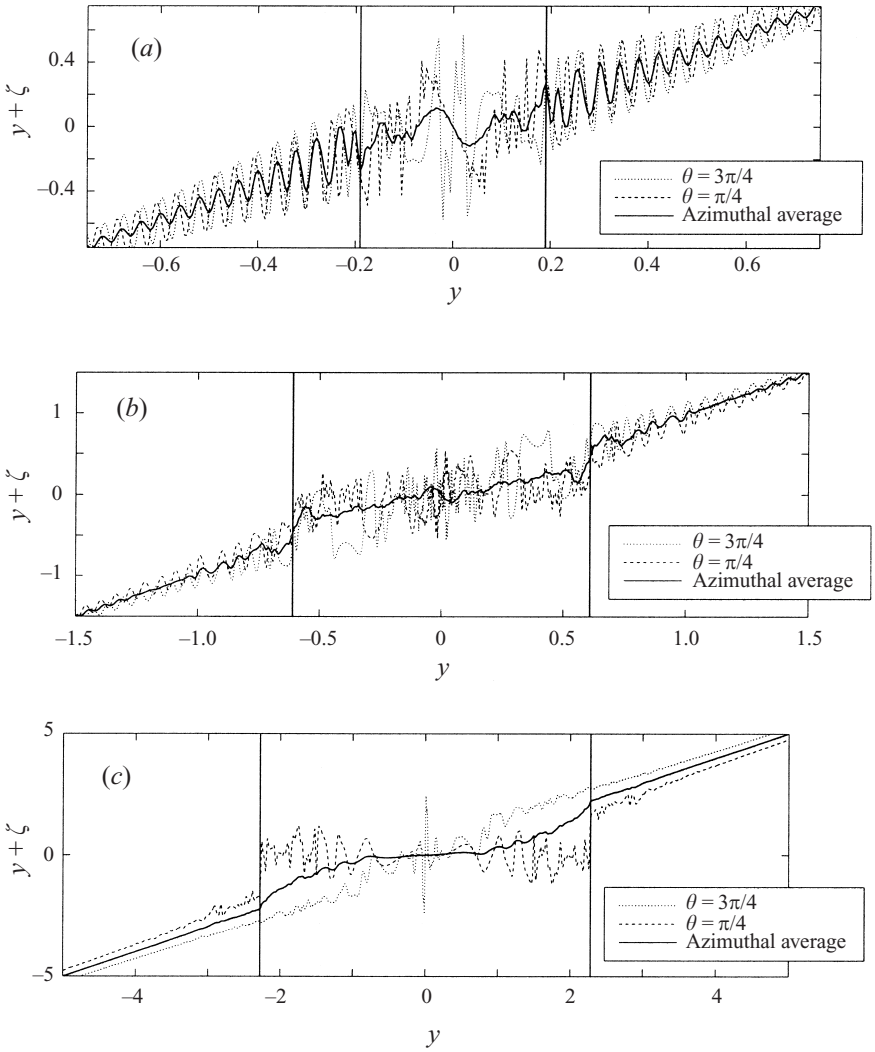


FIGURE 17. Radial slices of the vorticity field, $y + \zeta$, at fixed azimuthal angle for (*a*) $\chi = 0.272\chi_2$, (*b*) $\chi = 0.544\chi_2$, and (*c*) $\chi = 2.72\chi_2$, with $T = 1$. These snapshots are taken at $t = 90$ for (*a*), and $t = 60$ for (*b*) and (*c*). The vertical solid lines show the estimated maximum thickness of the cat's eye. Note that the horizontal scale changes in each panel, and the entire domain is not shown.

in figure 18, which shows a snapshot at $t = 40$ of a solution computed for the $\chi = 2.5\chi_1(t)$ case with $T = 1$. At this time, the vorticity has been wrapped into a fairly tight spiral inside the cat's eye, and the outer vorticity field is completely sheared out (the numerical integration has smoothed over much of this structure). However, the plot of $q = \zeta + y$ against ψ shows two populations of points. The first population lies outside and near the separatrix of the cat's eye (see panel *c*). This population has a ψ, q relation much like (6.17) for the passive scalar problem. (The relation (6.17) is also drawn in the figure together with the initial condition, $\psi = -q^2/2$.) The second population consists of points lying near the centre of the cat's eye (panel *b*). This second population, though far from its final state, appears to be converging towards the coarse-grained average, $q = \zeta + y = 0$, demanded by the symmetry of the initial condition.

https://doi.org/10.1017/S0022112000002159 Published online by Cambridge University Press

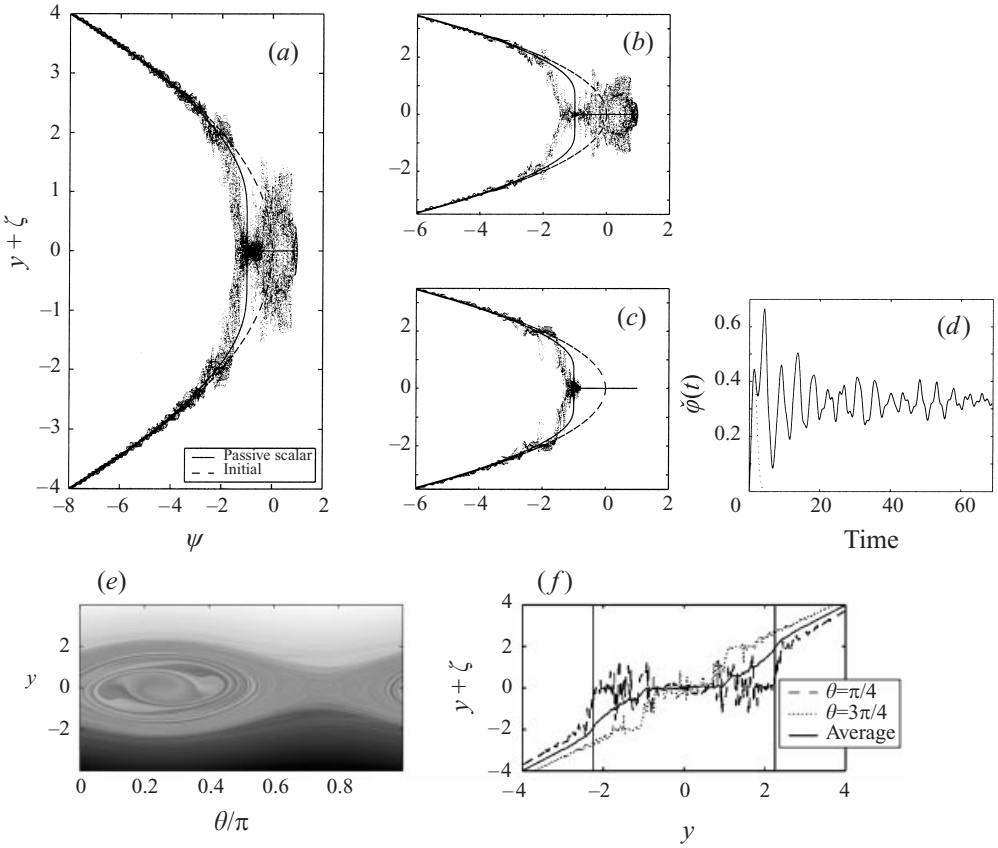


FIGURE 18. (*a*) Plots of ψ against $y+\zeta$ for $\chi = 2.5\chi_1(t)$ with $T = 1$, at time $t = 40$. In (*b*), we plot ψ, q points only for the region with $0.1 < \theta/\pi < 0.39$, which corresponds to a section encompassing the centre of the cat's eye. (*c*) A similar picture for $0.66 < \theta/\pi < 0.86$, which contains the hyperbolic point of the separatrices. Also plotted in (*a*)–(*c*) are the q, ψ relations for the initial condition (the dashed parabola) and the passive scalar solution, which is the solid curve. The solid passive-scalar curve consists of two branches: the curve given by (6.17) and a straight-line segment on which $y+\zeta = 0$. (*d*)–(*f*) Some further features of the corresponding solution, namely the evolution of the streamfunction, the vorticity distribution at $t = 40$, and radial slices through the total vorticity (with similar conventions to previous figures).

8. Conclusions

Our asymptotic analysis takes advantage of the fact that nearly compact, stable vortices have a special sensitivity to external perturbations. Specifically, the scaling of the external perturbation is taken to be order ϵ^3, yet the response of the quasi-mode is order ϵ^2. This is a kind of resonance, and requires that the external forcing has frequency content matching the rotation frequency of the quasi-mode. The forcing also excites further non-resonant disturbances, but these lie at higher order in our asymptotic scheme. In linear theory, these terms decay algebraically and have been identified by Bassom & Gilbert. Thus, the linear solution is summarized schematically in the formula

$$\psi = \epsilon^2(\text{exponentially decaying quasi-mode}) + \epsilon^3(\text{algebraically decaying contributions}). \quad (8.1)$$

https://doi.org/10.1017/S0022112000002159 Published online by Cambridge University Press

	$p=0$	$p=1$	$p=2$
$\omega_2/Z_{\max}$	$1/4$	0.185	0.158
r_2/R_C	$\sqrt{2}$	1.162	1.027
$R_C Z_{\max} \mathscr{I}_1$	$16\sqrt{2}=22.63$	38.45	63.23
$\lvert\mathscr{I}_5\rvert/R_C$	$4\sqrt{2}=5.657$	4.647	4.107
$\gamma/Z_{\max}$	$\pi\sqrt{2}/16\Upsilon=0.278\Upsilon$	$0.2205\ \Upsilon$	$0.1571\ \Upsilon$
v_c-1	$\Upsilon^2 A_c$	$1.187\ \Upsilon^2 A_c$	$1.027\ \Upsilon^2 A_c$

TABLE 2. Numerical values of ω_2, r_2, and of the integrals $\mathscr{I}_1$ and $\mathscr{I}_5$ in (3.23) for the first three members ($p=0$, 1 and 2) of the compact family in (2.3). The Landau damping rate, γ in (5.6), and the critical threshold of initial aspect ratio, v_c in (C 5) are also shown. The nondimensional parameter $\Upsilon \equiv R_C|\epsilon Z_S'(r_2)|/Z_{\max}$ measures the strength of the perturbation relative to the underlying compact vortex. Using figure 13, our best estimate of A_c in the bottom row of the table is $A_c \approx 0.9$.

Consequently, there is a switch-over from an initial exponential decay to a much slower algebraic decay for times of order $\log(1/\epsilon)$. The computations in Schecter *et al.* (1999) and Schecter (1999) display this exchange of order. We can summarize the linear theory by saying that in almost all circumstances axisymmetrization occurs. Exceptions to the previous statement are provided by vortices which for one reason or another possess undamped Kelvin modes. Into this category fall all contour dynamical simulations which employ discontinuous vorticity profiles.

The effect of nonlinearity is to slow the decay of the quasi-mode, or even arrest that decay if the initial amplitude of excitation exceeds a threshold. Above the threshold, cat's eye structures form, and, in the case of an $m=2$ perturbation, the result is a tripolar vortex, as seen in experiments. Because the forcing is scaled to be order ϵ^3, this threshold is actually small. Thus, finite-amplitude cat's eyes are the generic outcome of resonantly exciting the quasi-mode of the vortex.

We now use the family of compact vortices defined in (2.3) to estimate the dimensional Landau damping rate and the critical forcing threshold for the Gaussian vortex $Z_G = Z_{\max}\exp(-r^2/R_G^2)$. To ensure that the compact approximant has the same circulation as the Gaussian vortex, we use the relation (2.6) to determine R_C. The Landau damping rate, γ, is given in (5.6), and has the form of the dimensionless skirt vorticity gradient evaluated at the critical layer, $\Upsilon \equiv R_C|\epsilon Z_S'|/Z_{\max}$, multiplying a profile-dependent numerical coefficient, which is given in table 2. For the Gaussian, $\Upsilon = 2\sqrt{2}\mathrm{e}^{-2}$, 0.3125 and 0.2608 for $p=0$, 1 and 2, respectively. Hence, $\gamma/Z_{\max} \approx 0.1063$, 0.069 and 0.041 in the three cases. This should be compared with the numerical result for the Gaussian presented by Schecter *et al.* (1999): $\gamma/Z_{\max} \approx 0.079$. The damping rate for the case $p=0$ is known analytically, namely $\gamma/Z_{\max} = (\pi\,\mathrm{e}^{-2}/4)$, and coincides with an earlier perturbation result quoted by Schecter *et al.* (1999). This agreement is rough, and surprisingly, the $p=1$ vortex gives a better estimate than $p=2$.

To express the critical threshold in a more useful form, we specialize to instantaneous kicks and convert $A_c(T=0) \approx 0.9$ into a critical initial aspect ratio of the perturbed vortex, as described in Appendix C. A perturbed vortex whose initial aspect ratio is greater than v_c will not return to axisymmetry. Instead, the nonlinear terms result in the formation of a permanent cat's eye structure. In Appendix C, we find that $v_c - 1 \propto \Upsilon^2$, with numerical constants of proportionality as given in table 2. Again, for the Gaussian, we have $v_c - 1 \approx 0.1318$, 0.1043, 0.0625 for the three values $p=0$, 1 and 2. These estimates indicate that, without viscosity, 5 or

https://doi.org/10.1017/S0022112000002159 Published online by Cambridge University Press

10% departures from axisymmetry are sufficient to prevent axisymmetrization of an elliptical Gaussian vortex.

We expect that the reduced system (3.35)–(3.37) is broadly applicable as a model of linear and weakly nonlinear relaxation in ideal plasmas and fluid shear flows. In analogy with plasma physics, one might call this system the 'single-wave model'.

The view here is that if ϵ is small, so that a vortex is approximated by a compact vortex, then the single-wave model describes the weakly nonlinear evolution of the most easily excited perturbations on this vortex. Moreover for a certain class of $m = 2$ perturbations we have calculated the critical initial aspect ratio for return to axisymmetry.

This work was supported by the National Science Foundation (grant number OCE9529 824), and partly carried out at the 1999 Geophysical Fluid Dynamics Summer Study Program, Woods Hole Oceanographic Institution. S. G. L. S. was supported by a Research Fellowship from Queens' College. N. J. B. acknowledges an equipment grant from the Nuffield Foundation. We thank A. Bernoff and the anonymous referees for helping to improve the manuscript.

Appendix A. Computational technicalities

When written in terms of $F = \zeta + \beta y$, the equation for ζ reduces to the advection-diffusion equation $F_t + yF_\theta + \varphi_\theta F_y = 0$. ($F$ can be used instead of ζ interchangeably in the $\langle\,\rangle$ term since $\langle y\rangle = 0$.) We solve the equations with an operator splitting scheme based on the algorithm developed by Cheng & Knorr (1976) for the Vlasov equation (see also Feix *et al.* 1994), and subject to the boundary condition in y: $\zeta \to 0$ as $y \to \pm\infty$. In order to save computing the evolution of unneeded angular harmonics, we consider a periodicity in θ of π rather than 2π.

A.1. *Asymptotic solutions for large y*

To avoid dealing with an infinite domain, we truncate the range in y and solve the vorticity equation over the region $-L < y < L$. This requires boundary conditions at $y = \pm L$. To increase the accuracy of this truncation of the domain, we use the asymptotic solution for large y: to order L^{-3},

$$\zeta \sim \zeta_a = -\frac{\varphi}{y} + \frac{1}{2y^2}[\chi(0)\mathrm{e}^{2\mathrm{i}(\theta - yt)} + \text{c.c.}] - \frac{1}{4y^2}\varphi_{t\theta}. \tag{A 1}$$

The slow algebraic decay of the vorticity complicates the numerical scheme over the original Cheng & Knorr algorithm.

A.2. *Operator splitting*

We divide an integration step over the interval $[t, t+\tau]$ into three stages:

A.2.1. *Advect in θ for half a time step*

This amounts to solving

$$F_t + yF_\theta = 0 \tag{A 2}$$

over $[t, t+\tau/2]$, leaving $\hat{\varphi}$ unchanged. The exact solution is $F^\alpha(y,\theta) = F(y, \theta - y\tau/2, t)$. This shift in θ is computed using Fourier interpolation.

https://doi.org/10.1017/S0022112000002159 Published online by Cambridge University Press

A.2.2. *Advect in y for a complete time step*

We then solve

$$F_t - 4(\hat{\varphi}_r \sin 2\theta - \hat{\varphi}_i \cos 2\theta)F_y = 0 \tag{A 3}$$

and

$$\mathrm{i}\hat{\varphi}_t = \chi + \langle \mathrm{e}^{-2\mathrm{i}\theta} F \rangle \tag{A 4}$$

for $[t, t+\tau]$, where $\hat{\varphi}(t) = \hat{\varphi}_r(t) + \mathrm{i}\hat{\varphi}_i(t)$. Because the advection in y amounts to a shift of that coordinate, the integral in $\langle \mathrm{e}^{-2\mathrm{i}\theta} F \rangle$ does not change during y-advection. Hence we can deal with the equation for $\hat{\varphi}$ independently of the abridged vorticity equation. We do this by explicitly isolating the part of the integral over the computational domain, $-L < y < L$, from the part that originates outside. We approximate the latter using the large-y theory (Haynes 1985). Hence,

$$\langle \mathrm{e}^{-2\mathrm{i}\theta} F \rangle = \langle \mathrm{e}^{-2\mathrm{i}\theta} F \rangle_L - \frac{\mathrm{i}}{L}\hat{\varphi}_t + \frac{1}{L}\chi(0)\mathscr{F}(2Lt) + O(L^{-2}), \tag{A 5}$$

where

$$\mathscr{F}(X) = \int_1^\infty \cos(X\eta)\frac{\mathrm{d}\eta}{\eta^2}, \tag{A 6}$$

and $\langle\ \rangle_L$ has the obvious meaning. Hence,

$$\mathrm{i}(1 + L^{-1})\hat{\varphi}_t = \chi + \langle \mathrm{e}^{-2\mathrm{i}\theta} F \rangle_L + \frac{1}{L}\chi(0)\mathscr{F}(2Lt) + O(L^{-2}). \tag{A 7}$$

But $\langle \mathrm{e}^{-2\mathrm{i}\theta} F \rangle_L$ is constant over the step, and so

$$\begin{aligned} &\mathrm{i}(1 + L^{-1})[\hat{\varphi}(t+\tau) - \hat{\varphi}(t)] \\ &\qquad = \tau\langle \mathrm{e}^{-2\mathrm{i}\theta} F \rangle_L + \int_t^{t+\tau} \left[\chi(s) + \frac{1}{L}\chi(0)\mathscr{F}(2Ls)\right] \mathrm{d}s + O(\tau L^{-2}). \end{aligned} \tag{A 8}$$

Now we solve the y-advection equation: $F^\beta(y,\theta) = F^\alpha(y - V\tau, \theta)$, where $V = -4(\bar{\varphi}_r \sin 2\theta - \bar{\varphi}_i \cos 2\theta)$, and $\bar{\varphi}_r = [\hat{\varphi}_r(t+\tau) + \hat{\varphi}_r(t)]/2$ and $\bar{\varphi}_i = [\hat{\varphi}_i(t+\tau) + \hat{\varphi}_i(t)]/2$ are averages over the step. The introduction of these averages ensures second-order accuracy in time.

We accomplish the shift in y using interpolation with cubic splines. (Cubic splines are also used to compute the integrals in $\langle \mathrm{e}^{-2\mathrm{i}\theta} F \rangle_L$.) The interpolation can be performed as long as the shifted position, $-V\tau$, lies inside the computational domain. However, for the boundary points, $-L - V\tau$ lies below the domain if $V > 0$, and $L - V\tau$ is above if $V < 0$. At these locations, we cannot use interpolation; the physical significance is that fluid is being advected into the domain from outside. Instead we fix the values of $F = \zeta + \beta y$ at these points according to the solution for large $|y|$ in (A 1).

A.2.3. *Advect in θ for another half time step*

Finally, we again advect in θ. This gives $F(y, \theta, t+\tau) = F^\beta(y, \theta - y\tau/2)$ as the new vorticity distribution. Except at the first and final time steps, we can combine this step with the first one and shift in θ only once per time step.

A.3. *Choice of time step*

The main practical limitation on the time step (other than $\tau \ll 1$ for the sake of precision) is that we cannot shift in y over more than one grid point. Otherwise, fluid

https://doi.org/10.1017/S0022112000002159 Published online by Cambridge University Press

from outside invades our computational domain beyond one mesh point. Whilst this could easily be taken into account by using the asymptotic solution at the infected grid points, it signifies that accuracy is likely to be affected if the invasion becomes substantial. To avoid this situation, we limit the time step to ensure that shifts over more than one grid point do not take place.

With this limitation,

$$\Delta_y > \tau V_{\max} \equiv 4\tau|\hat{\varphi}|, \tag{A 9}$$

where Δ_y is the grid size in y. This leads us to choose a variable time step,

$$\tau(t) = \mathrm{Min}\left[\frac{3\Delta_y}{16|\hat{\varphi}(t)|}, \tau_{\max}\right], \tag{A 10}$$

where the arbitrary factor of $3/4$ ensures we do not violate (A 9), and the upper limit, $\tau_{\max}$, ensures we do not take an excessively long step. Note that there is no attempt to limit the amount of advection in θ.

In practice, for low-amplitude or short runs, we take $\tau_{\max} = 5 \times 10^{-3}$. In longer runs with large-amplitude streamfunctions, we take $\tau_{\max}$ as low as 10^{-4} to improve precision.

A.4. *Further details*

We have used various tests (doubling the grid size or maximum time step) to assess the accuracy of the scheme. Based on these tests, we used the following recipe. We choose a computational grid of size $(N, 2M+1)$ to cover the interval $0 \leqslant \theta \leqslant \pi$ and $-L \leqslant y \leqslant L$. We use $L = 5$ or 10, $N = 512$ and $M = 2000$ or 4000 for the large-amplitude runs in which we study the cat's eyes. For the lower-amplitude runs in which we compute the first bounce time, we use $L = 10$, $N = 32$ and $M = 4000$.

Spatial resolution is ultimately inadequate because of the increasing crenellation of the vorticity distribution. The finite resolution provides a numerical smoothing of the solution by which small-scale structure is lost, as shown by the comparison of exact and numerical solutions in figure 7.

The main effect of the finite L is to introduce spurious, low-amplitude oscillations into the streamfunction. These are evident in the two panels of figure 5, and obscure the ultimate decay of $\varphi(t)$ in the cases in which cat's eyes do not form. The frequency and amplitude of the oscillations is determined by L and the magnitude of $\chi'(0)$; we attempted to choose L to minimize any effect of this spurious ringing, whilst retaining adequate spatial resolution.

Appendix B. The correction $\breve{\varphi}_1(t)$ to the strongly forced limit

The expression (6.5) is obtained by multiplying the vorticity equation by y, spatially averaging and integrating in time. In the notation of § 6.2, the resulting integral is

$$\breve{\varphi}_1(t) = \tfrac{1}{2}\langle y\zeta_0(\theta, y, t)\rangle = \frac{1}{2}\int_{-\infty}^{\infty} \mathrm{d}y \oint \frac{\mathrm{d}\theta}{2\pi} y[y_0(\xi, y, t) - y]. \tag{B 1}$$

By symmetry, we need only consider $y > 0$ and $-\pi/2 < \xi < \pi/2$. The separatrix $m = 1$ divides the flow into two regions: one inside the cat's eye with $m > 1$ and one outside with $m < 1$.

Outside the cat's eye, we change variables from (ξ, y) to (u, m) where

$$\sin\xi = \mathrm{sn}(u; m), \qquad y = \frac{2}{\sqrt{m}}\,\mathrm{dn}(u; m) \tag{B 2}$$

https://doi.org/10.1017/S0022112000002159 Published online by Cambridge University Press

and

$$m = \frac{4}{y^2 + 4\sin^2\xi}\,. \tag{B 3}$$

The Jacobian of this transformation is $\partial(\xi, y)/\partial(u, m) = -2m^{-3/2}$. The range of integration becomes $0 < m < 1$ and $-\mathrm{K}(m) < u < \mathrm{K}(m)$, so the resulting subintegral is

$$I_1 = \frac{8}{\pi}\int_0^1 \frac{\mathrm{d}m}{m^{5/2}} \int_{-\mathrm{K}(m)}^{\mathrm{K}(m)} \mathrm{dn}(u;m)[\,\mathrm{dn}(u_0;m) - dn(u;m)]\,\mathrm{d}u, \tag{B 4}$$

where $u_0 = u - 2t/\sqrt{m}$. The orientation of the mapping $(\xi, y) \to (u, m)$ has been used to obtain the correct sign of I_1.

Now $\mathrm{dn}(u, m)$ may be expanded using

$$\mathrm{dn}(u, m) = \frac{\pi}{\mathrm{K}(m)}\left[\frac{1}{2} + 2\sum_{n=1}^{\infty} \frac{\varpi^n}{1+\varpi^{2n}} \cos(n\pi u/\mathrm{K})\right] \tag{B 5}$$

and substituted into I_1. The quantity

$$\varpi(m) \equiv \exp\left[-\pi\frac{\mathrm{K}(1-m)}{\mathrm{K}(m)}\right] \tag{B 6}$$

(usually denoted by q) is known as the nome. Orthogonality of trigonometric functions leads to the result

$$I_1 = -32\pi \int_0^1 \frac{\mathrm{d}m}{m^{5/2}\mathrm{K}(m)} \sum_{n=1}^{\infty} \frac{\varpi^{2n}}{(1+\varpi^{2n})^2} \left\{1 - \cos\left[\frac{2\pi n t}{\sqrt{m}\mathrm{K}(m)}\right]\right\}. \tag{B 7}$$

Inside the cat's eye, Jacobi's transformation may be used to transform from (ξ, y) to (v, m) by

$$\sin\xi = \frac{1}{\sqrt{m}}\,\mathrm{sn}(v; m^{-1}), \qquad y = \frac{2}{\sqrt{m}}\,\mathrm{cn}(v; m^{-1}), \tag{B 8}$$

which leads to $\partial(\xi, y)/\partial(v, m) = -2m^{-2}$. This mapping has negative orientation and the resulting subintegral is

$$I_2 = -\frac{8}{\pi}\int_1^{\infty} \frac{\mathrm{d}m}{m^3} \int_{-\mathrm{K}(m^{-1})}^{\mathrm{K}(m^{-1})} \mathrm{cn}(v; m^{-1})[\,\mathrm{cn}(v_0; m^{-1}) - \mathrm{cn}(v; m^{-1})]\,\mathrm{d}v, \tag{B 9}$$

where $v_0 = v - 2t$. The appropriate series to use now is

$$\mathrm{cn}(v, 1/m) = \frac{2\pi\sqrt{m}}{\mathrm{K}(m^{-1})} \sum_{n=1}^{\infty} \frac{\varpi^{n-1/2}}{1+\varpi^{2n-1}} \cos\left[\frac{(n+1/2)\pi v}{\mathrm{K}(m^{-1})}\right]. \tag{B 10}$$

Noting that $\varpi(m) = \varpi(m^{-1})$ and using orthogonality leads to

$$I_2 = 32\pi \int_1^{\infty} \frac{\mathrm{d}m}{m^2\mathrm{K}(m^{-1})} \sum_{n=1}^{\infty} \frac{\varpi^{2n+1}}{(1+\varpi^{2n+1})^2} \left\{1 - \cos\left[\frac{(2n+1)\pi t}{\mathrm{K}(m^{-1})}\right]\right\}. \tag{B 11}$$

Invoking the transformation $\mathrm{K}(m) = \mathrm{K}(m^{-1})/\sqrt{m}$ and taking $I_1 + I_2$ gives (6.3).

https://doi.org/10.1017/S0022112000002159 Published online by Cambridge University Press

Appendix C. The initial aspect ratio

For an impulsive kick with real amplitude B, the external forcing function in (3.5) is

$$\psi^{\rm ext} = 2r^2 B\delta(\tau)\cos 2\vartheta, \qquad \hat{b}(\tau) = B\delta(\tau). \tag{C 1}$$

The initial vorticity perturbation created by this kick is obtained from the balance

$$\zeta_\tau = \frac{1}{r}[Z_{\rm C}' + \epsilon Z_{\rm S}']\psi_\theta^{\rm ext} = -4rB[Z_{\rm C}' + \epsilon Z_{\rm S}']\delta(\tau)\sin 2\vartheta \tag{C 2}$$

in (3.3). Hence, at $t = 0^+$, the total vorticity field is

$$\begin{aligned}\zeta^{\rm Total}(r,\theta,0^+) &= [Z_{\rm C}(r) + \epsilon Z_{\rm S}(r)] - 4\epsilon^2 rB\sin 2\vartheta[Z_{\rm C}(r) + \epsilon Z_{\rm S}(r)]' + O(\epsilon^3)\\ &\equiv Z_{\rm C}(\kappa) + \epsilon Z_{\rm S}(\kappa) + O(\epsilon^3),\end{aligned} \tag{C 3}$$

where $\kappa = r - 4\epsilon^2 rB\sin 2\vartheta$. The impulsive kick therefore deforms the vortex elliptically and the ratio of major and minor axes is given by

$$v = \frac{1 + 4\epsilon^2|B|}{1 - 4\epsilon^2|B|} \approx 1 + 8\epsilon^2|B|. \tag{C 4}$$

We can relate B and A through the third relation in (3.34), and so

$$v = 1 + 8\epsilon^2 \frac{\mathscr{I}_1 r_2 \mathscr{L} A}{|\mathscr{I}_5|\mathscr{T}}. \tag{C 5}$$

The final line in table 2 is calculated using (C 5) after evaluating $\mathscr{I}_1$ and $\mathscr{I}_5$. To determine the critical aspect ratio from the calculations in § 7 we take the limit $T \to 0$ so that $\chi \to A\delta(t)$. This corresponds to extrapolating the curves in figure 13 to $T = 0$, which gives $A_c \approx 0.9$.

REFERENCES

Abramowitz, M. & Stegun, I. 1972 *Handbook of Mathematical Functions*. Dover.

Balmforth, N. J. 1998 Stability of vorticity defects in viscous shear. *J. Fluid Mech.* **357**, 199–224.

Balmforth, N. J., del-Castillo-Negrete, D. & Young, W. R. 1997 Dynamics of vorticity defects in shear. *J. Fluid Mech.* **333**, 197–230.

Bassom, A. P. & Gilbert, A. D. 1998 The spiral wind-up of vorticity in an inviscid planar vortex. *J. Fluid Mech.* **371**, 109–140.

Batchelor, G. K. 1967 *An Introduction to Fluid Dynamics*. Cambridge University Press.

Benney, D. J. & Bergeron, R. F. 1969 A new class of nonlinear waves in parallel flows. *Stud. Appl. Maths* **48**, 181–204.

Bernoff, A. J. & Lingevitch, J. 1994 Rapid relaxation of an axisymmetrical vortex. *Phys. Fluids* **6**, 3717–3723.

Bernstein, I. B., Greene, J. M. & Kruskal, M. D. 1958 Exact nonlinear plasma oscillations. *Phys. Rev.* **108**, 546–550.

Briggs, R. J., Daugherty, J. D. & Levy, R. H. 1970 Role of Landau damping in crossed-field electron beams and inviscid shear flows. *Phys. Fluids* **13**, 421–432.

Cass, A. C. 1998 Experiments on Vortex Symmetrization in magnetized electron plasma columns. PhD thesis, University of California, San Diego.

Cheng, C. Z. & Knorr, G. 1976 The integration of the Vlasov equation in configuration space. *J. Comput. Phys.* **22**, 330–351.

Churilov, S. M. & Shukhman, I. G. 1987 The nonlinear development of disturbances in a zonal shear flow. *Geophys. Astrophys. Fluid Dyn.* **38**, 145–175.

del-Castillo-Negrete, D. 1998 Weakly nonlinear dynamics of electrostatic perturbations in marginally stable plasmas. *Phys. Plasmas* **5**, 3886–3900.

https://doi.org/10.1017/S0022112000002159 Published online by Cambridge University Press

Driscoll, C. F. & Fine, F. S. 1990 Experiments on vortex dynamics in pure electron plasma. *Phys. Fluids* B **2**, 1359–1366.

Dritschel, D. G. 1998 On the persistence of non-axisymmetric vortices in inviscid two-dimensional flows. *J. Fluid Mech.* **371**, 141–155.

Feix, M. R., Bertrand, P. & Ghizzo, A. 1994 Eulerian codes for the Vlasov equation. In *Advances in Kinetic Theory and Computing* (ed. B. Perthame), pp. 45–81. World Scientific.

Goldstein, M. E. & Hultgren, L. S. 1988 Nonlinear spatial evolution of an externally excited instability wave in a free shear layer. *J. Fluid Mech.* **197**, 259–330.

Goldstein, M. E. & Leib, S. J. 1988 Nonlinear roll-up of externally excited free shear layers. *J. Fluid Mech.* **191**, 481–515.

Gould, R. W. 1994 Dynamics of non-neutral plasmas. *Phys. Plasmas* **2**, 2151–2163.

Haynes, P.H. 1985 Nonlinear instability of a Rossby-wave critical layer. *J. Fluid Mech.* **161**, 493–511.

Heijst, G. J. F. van, Kloosterziel, R. C. & Williams, C. W. M. 1991 Laboratory experiments on the tripolar vortex in a rotating fluid. *J. Fluid Mech.* **225**, 301–331.

Imamura, T., Sugihara, R. & Taniuti, T. 1969 An asymptotic method for the Vlasov equation. *J. Phys. Soc. Japan* **27**, 1623–1630.

Kelvin, Lord 1880 On the vibrations of a columnar vortex. *Phil. Mag.* **10**, 155–168.

Killworth, P. D. & McIntyre, M. E. 1985 Do Rossby-wave critical layers absorb, reflect or over-reflect? *J. Fluid Mech.* **161**, 449–492.

Kloosterziel, R. C. & Carnevale, G. F. 1999 On the evolution and saturation of instabilities of two-dimensional isolated circular vortices. *J. Fluid Mech.* **388**, 217–257.

Le Dizès, S. 2000 Non-axisymmetric vortices in two-dimensional flows. *J. Fluid Mech.* **406**, 175–198.

Lingevitch, J. F. & Bernoff, A. J. 1995 Distortion and evolution of a localized vortex in an irrotational flow. *Phys. Fluids* **7**, 1015–1026.

Manfredi, G. 1997 Long-time behaviour of nonlinear Landau damping. *Phys. Rev. Lett.* **79**, 2815–2819.

Möller, J. D. & Montgomery, M. T. 1999 Vortex Rossby waves and hurricane intensification in a barotropic model. *J. Atmos. Sci.* **56**, 1674–1687.

Montgomery, M. T. & Kallenbach, R. J. 1997 A theory for vortex Rossby waves and its application to spiral bands and intensity changes in hurricanes. *Q. J. R. Met. Soc.* **123**, 435–465.

O'Neil, T. M. 1965 Collisionless damping of nonlinear plasma oscillations. *Phys. Fluids* **8**, 2255–2262.

O'Neil, T. M.,Winfrey, J. H. & Malmberg, J. H. 1971 Nonlinear interaction of a small cold beam and a plasma. *Phys. Fluids* **14**, 1204–1212.

Rayleigh, Lord 1880 On the stability, or instability, of certain fluid motions. *Proc. Lond. Math. Soc.* **9**, 57–70.

Rhines, P. B. & Young, W. R. 1983 How rapidly is passive scalar mixed within closed streamlines? *J. Fluid Mech.* **133**, 133–145.

Rossi, L. F., Lingevitch, J. F. & Bernoff, A. J. 1997 Quasi-steady monopole and tripole attractors for relaxing vortices. *Phys. Fluids* **9**, 2329-2338.

Schecter, D. A. 1999 On the dynamics of inviscid relaxation in 2D fluids and nonneutral plasmas. PhD thesis, University of California, San Diego.

Schecter, D. A., Dubin, D. H. E., Cass, A. C., Driscoll, C. F., Lansky, I. M. & O'Neil, T. M. 1999 Inviscid damping of elliptical perturbations on a 2D vortex. In *AIP Proc. 1999 Non-neutral Plasmas Workshop*.

Stewartson, K. 1978 The evolution of the critical layer of a Rossby wave. *Geophys. Astrophys. Fluid Dyn.* **9**, 185–200.

Stewartson, K. 1981 Marginally stable inviscid flows with critical layers. *IMA J. Appl. Maths* **27**, 133–175.

Sugihara, R. & Kamimura, T. 1972 An asymptotic method for the Vlasov equation. III Transition from amplitude oscillations to linear Landau damping. *J. Phys. Soc. Japan* **33**, 206–215.

Tennyson, J. L., Meiss, J. D. & Morrison, P. J. 1994 Self-consistent chaos in the beam-plasma instability. *Physica* D **71**, 1–17.

Warn, T. & Gauthier, P. 1989 Potential vorticity mixing by marginally unstable baroclinic disturbances. *Tellus* **41A**, 115–131.

Warn, T. & Warn, H. 1978 The evolution of a nonlinear critical level. *Stud. Appl. Maths* **59**, 37–71.

https://doi.org/10.1017/S0022112000002159 Published online by Cambridge University Press